SET-UP AND EVALUATION OF LASER-DRIVEN MINIFLYER SYSTEM

A Thesis
Presented to
The Academic Faculty

by

Christopher W. Miller

In Partial Fulfillment
of the Requirements for the Degree
Master of Science in the
George W. Woodruff School of Mechanical Engineering

Georgia Institute of Technology
May 2009

SET-UP AND EVALUATION OF LASER-DRIVEN MINIFLYER SYSTEM

Approved by:

Professor Naresh Thadhani, Advisor
Materials Science and Engineering
Georgia Institute of Technology

Professor Suman Das
Mechanical Engineering
Georgia Institute of Technology

Dr. Mario Fajardo
Principal Research Chemist
US Air Force Research Laboratory

Professor Min Zhou
Mechanical Engineering
Georgia Institute of Technology

Date Approved: 1 April 2009

To my wife, Liz.

ACKNOWLEDGEMENTS

I want to thank Dr. Thadhani for guiding me through the creation of this thesis. Also, thanks to all of the members of the High Strain Rate Laboratory for providing insight and information during all stages of my graduate career and the writing of this thesis. Finally, I want to thank the members of my committee who set aside time to read and review my thesis–especially Mario Fajardo who traveled many miles for my oral presentation. Research was funded by ONR/MURI grants no. N00014-07-1-0740 and no. N00014-08-1-0982.

TABLE OF CONTENTS

DEDICATION iii

ACKNOWLEDGEMENTS iv

LIST OF TABLES vii

LIST OF FIGURES viii

SUMMARY xii

I INTRODUCTION 1

1.1 Research Motivation 1

1.2 Overview of Thesis 2

II BACKGROUND 3

2.1 Shock Physics Experiments 3

2.2 Laser-Driven Miniflyer System 8

2.3 Variables Influencing the Design of the Laser-Driven Miniflyer System 11

2.3.1 Window Materials 11

2.3.2 Substrate Window Coating and Flyer Material 13

2.3.3 Laser Fluence 16

2.3.4 Drive Laser Characteristics 22

2.4 Velocity Measurement Diagnostics 25

2.4.1 Photonic Doppler Velocimeter 27

III LASER-DRIVEN MINIFLYER SET-UP: LAYOUT AND COMPONENTS 31

3.1 Laser Drive Source 33

3.1.1 Drive Laser Characteristics 33

3.1.2 Laser-Drive Source Components 35

3.2 Substrate/Flyer Assembly 42

3.2.1 Window Material 42

3.2.2 Substrate Window Coatings 43

3.2.3 Flyer Material and Thickness 43
3.2.4 Substrate/Flyer Holder 44
3.2.5 Flyer-Target Impact Experiment Chamber 46
3.3 PDV Setup 48
IV REPRESENTATIVE MEASUREMENTS 52
4.1 Flyer Velocity Profiles 52
4.2 Effect of Driving Laser Energy 54
4.2.1 Conversion Efficiency 61
V SUMMARY OF RESULTS AND RECOMMENDATIONS 66
5.1 Results 66
5.2 Recommendations 67
APPENDIX A OPERATION MANUAL FOR LASER-DRIVEN MINIFLYER SYSTEM 70
REFERENCES 74

LIST OF TABLES

1 PDV primary components and vendors (Strand, 2005). 27

2 Average flyer mass, minimum launch energy and conversion efficiency for each flyer setup. 61

LIST OF FIGURES

1 An explosive plane-wave generator consisting of conical assembly of two explosives of different detonation velocity (Asay, 1993). 4

2 Schematic illustration of a gun experiment in which the projectile is accelerated using compressed gas or propellant to impact a target specimen. Impact velocities are measured using electrical probes or laser beam interruption (Asay, 1993). 5

3 A typical two-stage gas gun in which ignited gun powder drives a deformable plastic piston that compresses hydrogen or another light gas until a burst valve is released, accelerating the projectile. As the projectile begins its acceleration, the piston continues moving into a conical section of the acceleration reservoir where it is squeezed down by the cone picking up speed and pushing the rest of the hydrogen in the reservoir down the barrel to further accelerate the projectile (Asay, 1993). 6

4 A laser pulse travels through the uncoated side of a substrate transparent to the wavelength of the laser. The laser energy irradiates the carbon coating to create a plasma. The expanding plasma is thermally isolated from the flyer by the laser of aluminum oxide, and the layer of aluminum physically contains the plasma (Swift, 2005). 7

5 Flyer velocity profiles for 0.05 mm-thick copper flyers launched from four window materials (2.1 J for each shot) (Robbins, 2004). 12

6 Flyer velocity versus driving-laser pulse energy for (a) quartz and sapphire and (b) commercial-grade and laser-grade BK7 window materials (Robbins, 2004). 14

7 Peak flyer velocities as a function of incident fluence. Comparison of data with analytical model for aluminum and composite targets (Trott, 1994). 15

8 Comparison between various Al targets, showing the effect of a dielectric layer (Hatt, 1996). 16

9 Symmetrical sandwich configuration with center plane comprising of flat explosive layer of mass C and two flyer plates of mass M each, used to study the explosive-metal interaction and resulting acceleration of metal plates. 17

10 Exponential energy deposition profile (Lawrence, 1993). 19

11 Peak flyer velocities versus incident fluence for indicated foil thicknesses and laser pulse durations (Trott, 1991). 20

12 Peak flyer velocities versus laser energy with least squares fits assuming a square root dependence of foil velocity on laser energy (Trott, 1990). 21

13 Comparisons between theory and experiment for lens-coupled Al flyers (Lawrence, 1993). 22

14 Uniform irradiance obtained by aperturing input beam (Dickey, 2000). 23

15 Schematic layout of two-lens beam reshaping optics illustrating the (a) Galilean and (b) Keplerian geometries (Hoffnagle, 2003). 24

16 Beam intensity variations with changes in β (Romero, 1996). 25

17 A 110 Hz sine wave (cyan) beating with a 104 Hz sine wave (magenta) to create a beat frequency of 6 Hz (red). 26

18 The basic geometry of a PDV system (Strand, 2006). 28

19 The PDV system shown with three-port circulator, component vendors, and parts numbers (Strand, 2006). 29

20 Miniflyer system table layout 1: (1) 3 J Nd:YAG 1064 nm driving laser, (2) fiber optic coupled injection seeder laser, (3) 2.7 mW Diode 635 nm alignment laser, (4) Faraday isolator, (5) high-energy mirrors, (6) 8 mm aperture, (7) 250 mm focusing lens, (8) experiment chamber, (9) laser diagnostics. 32

21 Miniflyer system table layout 2: (1) 3 J Nd:YAG 1064 nm driving laser, (2) fiber optic coupled injection seeder laser, (3) 2.7 mW Diode 635 nm alignment laser, (4) Faraday isolator, (5) high-energy mirrors, (6) beam resizing optics, (7) refractive beam shaper, (8) 250 mm focusing lens, (9) experiment chamber, (10) laser diagnostics. 32

22 Gaussian beam profile of the driving laser. 34

23 Psuedo-top hat profile created by the 8 mm aperture. 34

24 Psuedo-top hat profile created by the refractive beam shaper. 35

25 The three components of a Faraday isolator (light traveling left to right). Light travels through easily. 37

26 The three components of a Faraday isolator (light traveling right to left). Light is blocked by the input polarizer. 38

27 The effects of lenses on the beam size. 39

28 Maximum laser energy versus FWHM laser energy. 41

29 An apparatus created to ensure that the marker spot is directly opposite of the flyer location. The marker is aligned with the small point of plastic on the bottom so that when the flyer is centered on the plastic point, the marker will mark this position on the other side of the substrate. 45

30 PMMA open air sample holder. 45

31 Single shot open air impact experiment chamber. 46

32 Impact experiment chamber designed to hold a vacuum. 47

33 Typical set of components as assembled inside vacuum chamber (Robbins, 2004. 47

34 Beam spot size at different distances from the focal lens. 48

35 PDV velocity curves with varying window sizes: (a) window = 3000 time points, (b) window = 6000 time points, (c) window = 12000 time points, (d) window = 25000 time points. 50

36 Velocity information is extracted by tracing the velocity curve. Data can be saved in ASCII format for analysis in Excel. 51

37 Flyer velocity versus laser pulse energy for 3.2 mm-diameter, 100 μm-thick flyer. Beam shaping done using an 8 mm aperture. 53

38 Flyer velocity versus laser pulse energy for 2.4 mm-diameter, 25 μm-thick flyer. Beam shaping done using an 8 mm aperture. 53

39 Velocity versus total distance traveled curves for $\sim$900 mJ shots on 3.2 mm- and 2.4 mm-diameter flyers of 100 μm, 50 μm, and 25 μm thickness. Beam shaping done using an 8 mm aperture. 55

40 Velocity versus distance traveled during initial launch curves for $\sim$900 mJ shots on 3.2 mm- and 2.4 mm-diameter flyers of 100 μm, 50 μm, and 25 μm thickness. Beam shaping done using an 8 mm aperture. . 56

41 Flyer velocity versus laser pulse energy for 3.2 mm-diameter flyers in three thicknesses: 100 μm, 50 μm, and 25 μm. Beam shaping done using an 8 mm aperture. 57

42 Flyer velocity versus laser pulse energy for 2.4-mm diameter flyers in three thicknesses: 100 μm, 50 μm, and 25 μm. Beam shaping done using an 8 mm aperture. 58

43 Flyer velocity versus laser pulse energy for 25 μm-thick flyers of 3.2- and 2.4 mm-diameter. Beam shaping done using an 8 mm aperture. . 59

44 Plots of flyer velocity versus laser pulse energy for 50 μm-thick, 3.2 mm-diameter flyers comparing beam shaping done with a refractive beam shaper and beam shaping done using an 8 mm aperture. 60

45 Plot of velocity versus the square root of laser pulse energy for 3.2 mm-diameter, 25 μm-thick flyers. A linear regression is used to find the conversion efficiency, k, for the system. 62

46 Plots of flyer velocity versus laser pulse energy with k curve fit for 3.2 mm-diameter flyers in three thicknesses: 100 μm, 50 μm, and 25 μm. Beam shaping done using an 8 mm aperture. 63

47 Plots of flyer velocity versus laser pulse energy with k curve fit for 2.4 mm-diameter flyers in three thicknesses: 100 μm, 50 μm, and 25 μm. Beam shaping done using an 8 mm aperture. 64

48 Conversion efficiency, k, for each flyer setup versus flyer thickness. Error is based on the farthest point from the linear fit to the plot of velocity versus square root of laser pulse energy. 65

SUMMARY

A laser-driven miniflyer system is built in design similar to those at the Los Alamos National Laboratory and Eglin Air Force Base. It is composed of three parts: laser drive source, impact experiment assembly, and diagnostics. The laser drive source is a Nd:YAG laser operating at 1064nm at a maximum energy of 3 J. The impact experiment assembly consists of a BK7 substrate on to which is deposited an ablation layer consisting of carbon, alumina, and aluminum. Mounted on the ablation layer is a metal foil (flyer). The carbon in the ablation layer absorbs the laser energy to form a rapidly expanding plasma. The alumina and aluminum layers provide thermal insulation and also contain the plasma. The set-up is expected to provide flyer velocities in the range of 100 to 1000 m/s. Diagnostics consist of a Photonic Doppler Velocimetry (PDV) system that uses Doppler-shifted coherent laser light to measure the instantaneous velocity of a moving surface, as well as velocity dispersions caused by mechanical or material heterogeneities. This thesis will provide a description of the set-up of the laser-driven miniflyer system, as well as an evaluation of the flyer velocity, measured using the PDV system, as a function of laser energy. The flyer velocity trends will be used in order to characterize and calibrate the system. A manual providing system operation instructions will also be included to serve future users of this miniflyer system.

CHAPTER I

INTRODUCTION

1.1 Research Motivation

The laser-driven miniflyer system was designed to augment experiments performed on gas guns, rail guns, powder guns and other large scale shock physics equipments. It has advantages compared to other types of shock physics and mechanics experiments because there is relatively little momentum or energy associated with the acceleration process, so the system can be significantly smaller and sample recovery can be significantly easier. It also reduces the cost per shot and enables repetitive experiments on a shorter timeline. It is possible to routinely achieve up to 20 high-quality experiments per day, compared with one or fewer on a gun. This, together with lower cost, makes it possible to address one of the chronic problems of shock experiments–a deficiency of repeat experiments and poorer statistics than in most other fields of physics. Laser-driven miniflyer experiments also make it more convenient to study small samples; a significant benefit when dealing with toxic, radioactive, or expensive materials, or for correlating with numerical simulations such that the experiment and simulation are performed at the same scale.

The motivation of this research is to set-up and characterize the performance of the laser-driven miniflyer system. Future experiments are dependent on the results of this research for the velocity versus laser pulse energy calibration curves generated in this work. Decisions on flyer diameter, thickness, and mass can be based on measured conversion efficiencies of each flyer setup, and spatial dimensions can be based on plots of velocity versus distance. This research provides the foundation for future research in high strain rate research and shock physics applications.

1.2 Overview of Thesis

A background on the history of shock physics experimental approaches will be provided followed by descriptions of existing laser-driven miniflyer systems and their uses. Variables that influence the design of the miniflyer system will be discussed as well as the diagnostic tools used to measure the flyer and particle velocities. The variables discussed in the background will then be addressed in a description of the experimental layout of the laser-driven miniflyer system. Also discussed will be the drive laser characteristics and the setup of the PDV system for diagnostics of flyer acceleration. Finally, an evaluation of velocity as a function of laser energy will be included in order to characterize the system. A manual providing system operation instructions will also be included to serve future users of this miniflyer system.

CHAPTER II

BACKGROUND

A review of previous studies relevant to the laser-driven miniflyer system will be presented in this chapter.

2.1 Shock Physics Experiments

In order to fully understand the conditions and reasoning for use of a laser-driven miniflyer system, it is important to understand the progression of shock physics experiments and their uses. The scientific basis for the description of solids under compression from strong shock waves was established with the review article published in the Solid State Physics Series by M.H. Rice, R.G. McQueen, and J.M. Walch of the Los Alamos Scientific Laboratory entitled "Compression of Solids by Strong Shock Waves" [25]. Since then, shock physics experiments have been developed for investigating the dynamic properties of materials such as the equation of state, strength, and phase changes. Shock compression is encountered when material bodies are subjected to loading in which the time of load application is short compared to the time for the body to respond inertially. The inertial responses are stress pulses propagating through the body to communicate the presence of loads to interior points [2].

Methods to generate planar shock compression are needed to study the Hugoniot, which relates the velocity of a shock wave and the pressure, density, and enthalpy of the transmitting solid before and after the shock wave passes. The methods also allow many other facets of a material's behavior under uniaxial strain loading to be studied. They can be divided into three categories: explosively-launched devices, gun-launched projectiles, and instantaneous energy deposition using lasers. Explosive launching with plane-wave generators require a design that makes use of the geometry

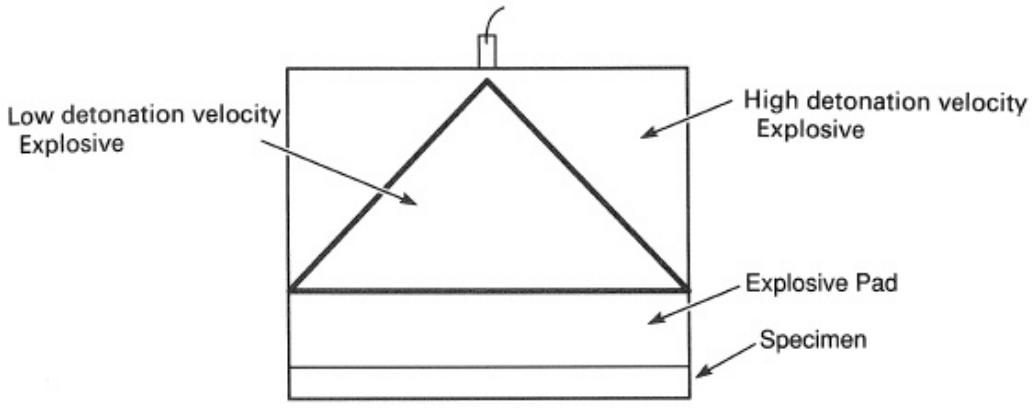

Figure 1: An explosive plane-wave generator consisting of conical assembly of two explosives of different detonation velocity (Asay, 1993).

which depends on differing detonation velocities in the system. This design produces a planar detonation front which initiates a planar shock front in the specimen of interest. One such plane-wave generating design is shown in Figure 1.

Planar shock waves can also be produced by using a gun to accelerate a flat-nosed projectile or flyer plate mounted on a sabot which then impacts on to a flat specimen (Figure 2). There are several types of guns. Each varies in that it uses a different kind of propelling medium to launch the projectile. Light gas guns use sudden release of compressed air or helium to shoot projectiles at speeds up to 1 $\frac{km}{s}$. Gas guns are useful for shock-wave experiments up to a few tens of GPa [1]. Powder guns use the energy released from high-pressure gases of the propellant products to accelerate the projectile to high velocities. Impact velocities to about 2.3 $\frac{km}{s}$ can be attained, generating peak shock pressures in materials to nearly 100 GPa [1].

Two-stage gas guns use ignited gun powder to drive a deformable plastic piston that compresses hydrogen or another light gas until a burst valve is released, thus accelerating the projectile. As the projectile begins its acceleration, the piston continues moving into a conical section of the acceleration reservoir. As the piston is squeezed down by the cone, it picks up speed and pushes the rest of the hydrogen in the reservoir down the barrel to further accelerate the projectile. Two-stage gas

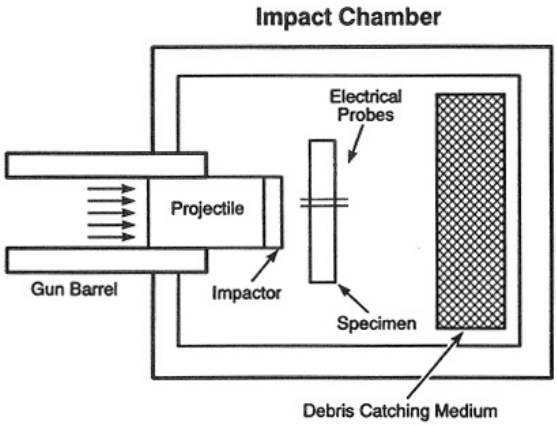

Figure 2: Schematic illustration of a gun experiment in which the projectile is accelerated using compressed gas or propellant to impact a target specimen. Impact velocities are measured using electrical probes or laser beam interruption (Asay, 1993).

guns are capable of attaining peak velocities in the 7-8 $\frac{km}{s}$ range with peak shock pressures approaching 1 TPa in high impedance materials [2]. The two-stage gas gun configuration is shown in Figure 3.

For velocities in the 10-20 $\frac{km}{s}$ range, a rail gun can be used. A rail gun consists of two parallel metal rails that are connected to an electrical power supply. When a conductive projectile is inserted between the rails it completes the circuit created by the two rails, and electrons are able to flow from the negative terminal of the power supply up the negative rail, across the projectile, and down the positive rail, back to the power supply. This current makes the rail gun behave similar to an electromagnet, creating a powerful magnetic field in the region of the rails up to the position of the projectile which accelerates the projectile along the rails. While velocities up to 20 $\frac{km}{s}$ are possible, the heat generated from the acceleration of the projectile can rapidly erode the rails. This requires frequent replacement of the rails, or use of a heat resistant material that is conductive enough to produce the same effect.

The directed energy deposition method describes the process used for the laser-driven miniflyer system. There are two techniques that can be used for flyer acceleration by a pulsed laser. The first is direct laser irradiation in which a thin foil flyer

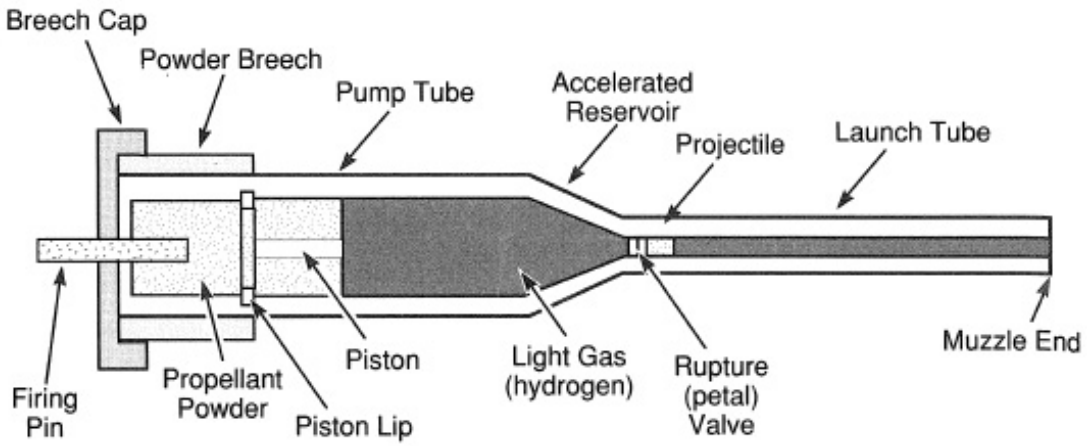

Figure 3: A typical two-stage gas gun in which ignited gun powder drives a deformable plastic piston that compresses hydrogen or another light gas until a burst valve is released, accelerating the projectile. As the projectile begins its acceleration, the piston continues moving into a conical section of the acceleration reservoir where it is squeezed down by the cone picking up speed and pushing the rest of the hydrogen in the reservoir down the barrel to further accelerate the projectile (Asay, 1993).

is directly irradiated by a laser beam and accelerated by the counterforce of the laser ablation. The unvaporized layer of foil is driven off as a flyer plate. He et al. [11] showed the acceleration of a 10 μm-thick Al foil up to 9.2 $\frac{km}{s}$ at a laser intensity of 260 $\frac{GW}{cm^2}$. This technique has very low efficiency during the energy conversion from laser energy to kinetic energy of the flyer because of the lack of a physical backing to contain the expanding plasma. Sheffield et al. [31] found efficiencies of less than 1% in experiments performed without a backing substrate.

The second technique remedies the low efficiency problem by using a plasma-confinement technique in which a composite foil is used rather than a single homogeneous foil. The foil is backed by a substrate to contain and direct the force of the plasma expansion. A three layer composite is used to thermally separate the plasma generating material from the flyer material (Figure 4). Often this middle layer is composed of a dielectric, such as aluminum oxide. Hongo et al. [14] used this technique to launch a 25 μm-thick Al flyer to 1.1 $\frac{km}{s}$ at a laser intensity of 4.9 $\frac{GW}{cm^2}$. This technique also detaches plate launch from plate impact. The shock generated in the target is

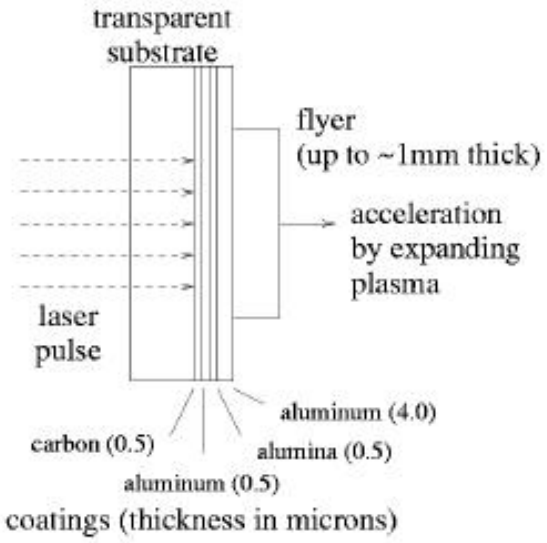

Figure 4: A laser pulse travels through the uncoated side of a substrate transparent to the wavelength of the laser. The laser energy irradiates the carbon coating to create a plasma. The expanding plasma is thermally isolated from the flyer by the laser of aluminum oxide, and the layer of aluminum physically contains the plasma (Swift, 2005).

decoupled from laser deposition and buffered from discontinuities in the laser beam profile [33].

The laser-driven miniflyer system has advantages compared to explosives and guns because there is relatively little momentum or energy associated with the acceleration process, so the apparatus can be significantly smaller and recovery of the sample significantly easier [38]. This reduces the cost per shot and enables repetitive experiments. Swift et al. [38] routinely achieve 10-15 high-quality experiments per day, compared with one or fewer on a gun, which, together with lower cost make it possible to address one of the chronic problems of shock experiments–a deficiency of repeat experiments and poorer statistics than in most other fields of physics. Laser-driven miniflyer experiments also make it more convenient to study small samples, a significant benefit when dealing with toxic, radioactive, or expensive materials.

It should be noted that laser generated shocks using large lasers have been used for many years to study material effects through direct laser-material interactions [21].

Rapid heating from the bombardment of photons on the target results in sudden expansion of the surface, creating a shock wave. Extreme conditions with shock pressures in the mega-bar range and strain rates $> 10^7$ s^{-1} are produced when the laser pulse ablates the target material producing a rapidly attenuating triangular shock-wave [16]. However, with such a loading condition, it is difficult to establish the true shock state and obtain correlation with resulting materials effects. The use of a laser pulse to produce a plasma to accelerate a flyer plate and impact a target provides much better definition and control of the shock pulse. The amplitude of the shock wave is governed by the impact velocity and the target-flyer material impedance, while the shock pulse duration is influenced by the thickness of the flyer plate. In a way, laser-accelerated flyer impacts represent a scaled-down version of gas gun plate-impact experiments, with shock pulses of nanosecond duration and strain rate of 10^6 s^{-1}.

2.2 Laser-Driven Miniflyer System

There are many types of laser-driven miniflyer systems in use around the world. Each has a setup that is tailored to the specific experiments it is used to perform. There are systems at Los Alamos National Laboratory, Air Force Research Laboratory at Eglin AFB, the Tokyo Institute of Technology, Sandia National Laboratories, the University of Tokyo, the Hebrew University of Jerusalem, and the University of Cambridge.

The miniflyer system at Los Alamos National Laboratory [27] is similar to the one being set up at the High Strain Rate Lab at the Georgia Institute of Technology. The driving laser used to launch the miniflyer is a single-shot, Q-switched Nd:glass laser consisting of an oscillator and up to two amplifiers. The oscillator produces a 20- or 40-ns pulse with a maximum energy of 3 J. With the two amplifiers, the final pulse can have up to 15 J of energy in a nearly Gaussian beam. This beam is focused into a top-hat profile using a diffractive beam shaper. A small portion (1%) of the

driving pulse is split off to a detector using a pellicle beam splitter.

Robbins et al. [27] mount each flyer plate on a 19 mm diameter by 1.6 mm thick substrate window coated with 0.5 μm layer of carbon, a 0.5 μm layer of aluminum oxide, and a 3.0 μm layer of aluminum. Mounted on the substrate with Epon Resin 815C with an RF20 hardener is a 3 mm diameter metal flyer. Typically, the flyers are 50 μm or 100 μm thick. A very small amount of glue is used (1 mL) to create a bond thickness on the order of 1 μm.

The Los Alamos setup uses VISAR to collect most of the miniflyer acceleration data [27]. Line optically recording velocity interferometer system (ORVIS) is also used for collecting data over a line rather than a single point. To measure the flyer plate behavior between launch and impact a stereoscopic camera system is used. Three-dimensional reconstructions of the flyer surface can be determined using this camera setup. The laser-driven miniflyer system at Los Alamos National Laboratory is used for copper and uranium spall measurements, as well as collecting Hugoniot data [27]. VISAR is used to measure the peak free-surface velocities of the materials to generate wave profiles. The wave profiles are then used to calculate spall strength and strain rate. To measure Hugoniot data using the miniflyer setup the change in velocity when the flyer impacted a window with known properties is observed. By measuring both the flyer velocity before impact and the flyer/window interface velocity after impact and knowing the window material's shock properties, a point on the Hugoniot can be determined [27].

The Tokyo Institute of Technology uses a Q-switched Nd:YAG laser with wavelength of 1064 nm and a pulse width of 10 ns. The Gaussian distribution of the laser beam is transformed to a flat-top profile with a multilens-array coupled with a planoconvex lens [14]. The focused laser spot is a hexagon with sides 1.25 mm long and a laser intensity between 2.0 and 4.9 $\frac{GW}{cm^2}$. Aluminum foil (10, 18, 25, 30, 40 or 50 μm thick) is glued to a 3 mm thick glass substrate using 5 μm of epoxy

resin. Shock compression and recovery experiments on MnF_2 are performed using the laser-accelerated flyer system with ORVIS used to measure free surface velocities of the flyer [14]. One of their experiments involves powdered MnF_2 compressed to 70% density and placed between a backup glass and aluminum pasted glass with a teflon spacer. The shock pressure from the impact of the flyer is obtained using an impedance matching method [14]. With this setup, Hongo et al [14] were able to accelerate the 25 μm thick aluminum flyer to 1.1 $\frac{km}{s}$ by laser irradiation at an intensity of 4.9 $\frac{GW}{cm^2}$. The resulting shock pressure was estimated to be 6.0 GPa [14].

Sandia National Laboratories uses a technique of fiber optic coupling rather than lens coupling [41]. The driving laser in this case is a Q-switched Nd:glass oscillator emitting light at 1054 nm in 18 ns pulses. Flyer targets are prepared using physical vapor deposition on polished output ends of 0.4 mm diameter multi-mode optical fibers [41]. The spatial profile of the laser is relatively flat at the output end of the fiber due to mode mixing of the laser within the fiber. ORVIS is used to determine velocity-time histories and final flyer velocities and an IMACON streak camera is used to capture images of accelerating flyers. The setup at Sandia is used for quantitative studies involving short-pulse shock compression.

Other laboratories use Nd:YAG lasers for studies of shock loading behavior. While the laser intensities that each laboratory uses may differ, the setups are very similar. A driving laser is sent through a beam shaper to create a top-hat profile [15] or left in its Gaussian form [11, 5, 43]. The beam then irradiates a metal foil or foil composite mounted on a glass substrate [15, 5, 43] creating a plasma that accelerates a portion of the foil towards a target. VISAR is used most often to determine flyer velocities [15, 11], but streak cameras are also used quite often [43, 11].

One notable difference in setup comes from Cogan et al. [5] at the Hebrew University of Jerusalem. In their setup, the laser beam is split so that the substrate is irradiated by two pulses with a predetermined time delay created by a three mirror

delay line [5]. The non-delayed beam is focused directly on the target while the delayed beam is incident on the target at 7° with respect to the normal. Measurements of the impact crater are done using a profilometer. These profilometric scans help to obtain a reliable estimate of the mass of the ejected flyer and therefore the launching efficiency of the laser system [5]. It was found that the delay leg decreased launching efficiency. Cogan et al. [5] concluded that the optimal pulse length would be in the subnanosecond region but above 20 ps.

2.3 Variables Influencing the Design of the Laser-Driven Miniflyer System

Many variables can influence the design and performance of the laser-driven miniflyer system. Among these are the substrate window materials used to mount the flyers, the substrate window coatings and flyer material, the laser fluence, and the drive laser characteristics. These variables will be discussed in the following sections.

2.3.1 Window Materials

The window material used as a substrate for the flyer assembly is a potentially significant parameter affecting flyer velocity. Paisley [23] used substrate windows to improve the coupling coefficient from the laser pulse to the flyer plate by confining the laser-beam side of the flyer plate with a high-impedance transparent material, rather than using direct irradiation methods. Robbins et al. [27] investigated the effects of four window materials: sapphire, fused silica, laser-grade BK7, and commercial grade BK7. All the materials are transparent to the 1054 nm wavelength light emitted from the Nd:Glass laser, but they have different refractive indices and different shock impedances. The refractive index is a measure of how much the speed of light is reduced inside the material. The shock impedance is the product of the density and the longitudinal wave speed. Sapphire has both the highest refractive index at 1.75 and the highest shock impedance at 45 $\frac{g}{cm^3}\frac{mm}{\mu s}$ [27]. Fused silica has the

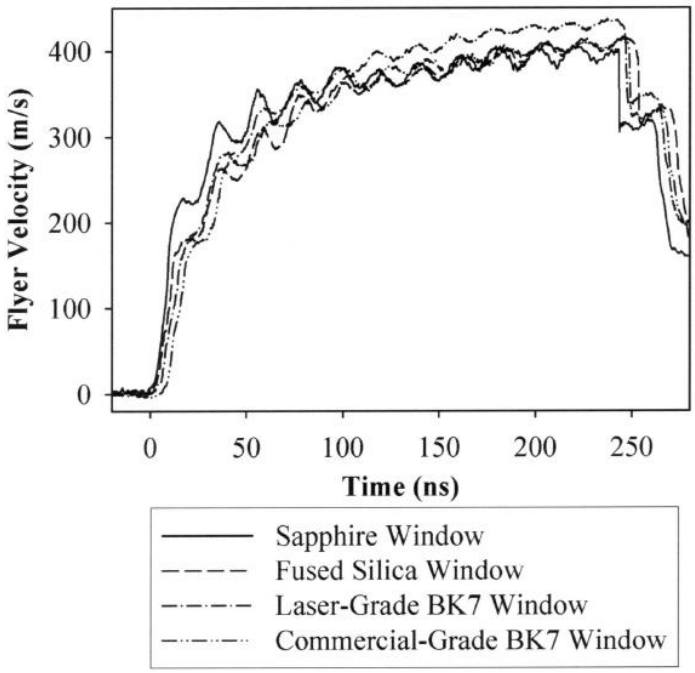

Figure 5: Flyer velocity profiles for 0.05 mm-thick copper flyers launched from four window materials (2.1 J for each shot) (Robbins, 2004).

lowest refractive index at 1.45 and a shock impedance of 13 $\frac{g}{cm^3}\frac{mm}{\mu s}$ [27]. BK7 has a refractive index of 1.51 and a shock impedance of 12 $\frac{g}{cm^3}\frac{mm}{\mu s}$ [27].

A set of flyer velocities for the four different window materials from Robbins et al. [27] is shown in Figure 5. Each flyer was launched with roughly 2.1 J per shot. The velocity versus time trends measured with VISAR are typical for these type of experiments. In fact, the results of tests by Stahl et al. [33] done with roughly 3.3 J per shot correspond very well to the tests done by Robbins et al [27]. Both research groups found that the flyer from the sapphire window achieved a slightly higher velocity at first, but its velocity leveled out sooner resulting in a slightly lower impact velocity [33, 27]. These results suggest that differences in window materials have little effect on impact velocities.

The amplitude of the oscillations in the velocity profiles does appear to be somewhat dependent on the window material. As seen in Figure 5, the amplitude of the oscillations was largest for the sapphire window due to the higher shock impedance

of sapphire [33]. The amplitudes of oscillation for the flyers launched off of the other window materials were lower by 25%-40% of that measured for the sapphire [27]. When considering the data for all of the experiments done by Robbins et al. [27], they found the same qualitative results leading to the conclusion that the difference is sufficiently small to be of little concern in choosing a window material.

Figure 6a and 6b show the primary results of the study by Robbins et al. [27]: the final flyer velocity versus pulse energy for all four of the window materials and both coating configurations (0.5 μm-thick Al vs. 5.0 μm-thick Al). A double exponential fit to the flyer velocity profile was used to determine the final flyer velocities. For the fused silica and sapphire windows (Figure 6a) the velocities are clustered, with up to +10% and -15% variation at a given pulse energy [27]. For the BK7 windows (Figure 6b), the clusters at a given pulse energy are much tighter, at most $\pm$5% variation and yield slightly higher velocities than the other windows [27]. Given the low cost of commercial-grade BK7 windows, Robbins et al. [27] used this material for all subsequent studies.

2.3.2 Substrate Window Coating and Flyer Material

As stated previously, there are two techniques that can be used for flyer acceleration by a pulsed laser. The first is direct laser irradiation in which a thin foil flyer is directly irradiated by a laser beam and accelerated by the counterforce of the laser ablation. In this case, the unvaporized layer of foil is driven off as a flyer plate. The second technique uses a composite material rather than a single homogeneous foil to better confine the plasma, create a thermal barrier, and increase the efficiency of the energy conversion from laser to kinetic energy of the flyer.

Studies by Trott [41] and Hatt et al. [10] both used homogeneous aluminum layers 4 μm thick to coat target substrates. These coatings were compared to composite coatings containing a sub-micron layer of aluminum oxide. The composite coatings

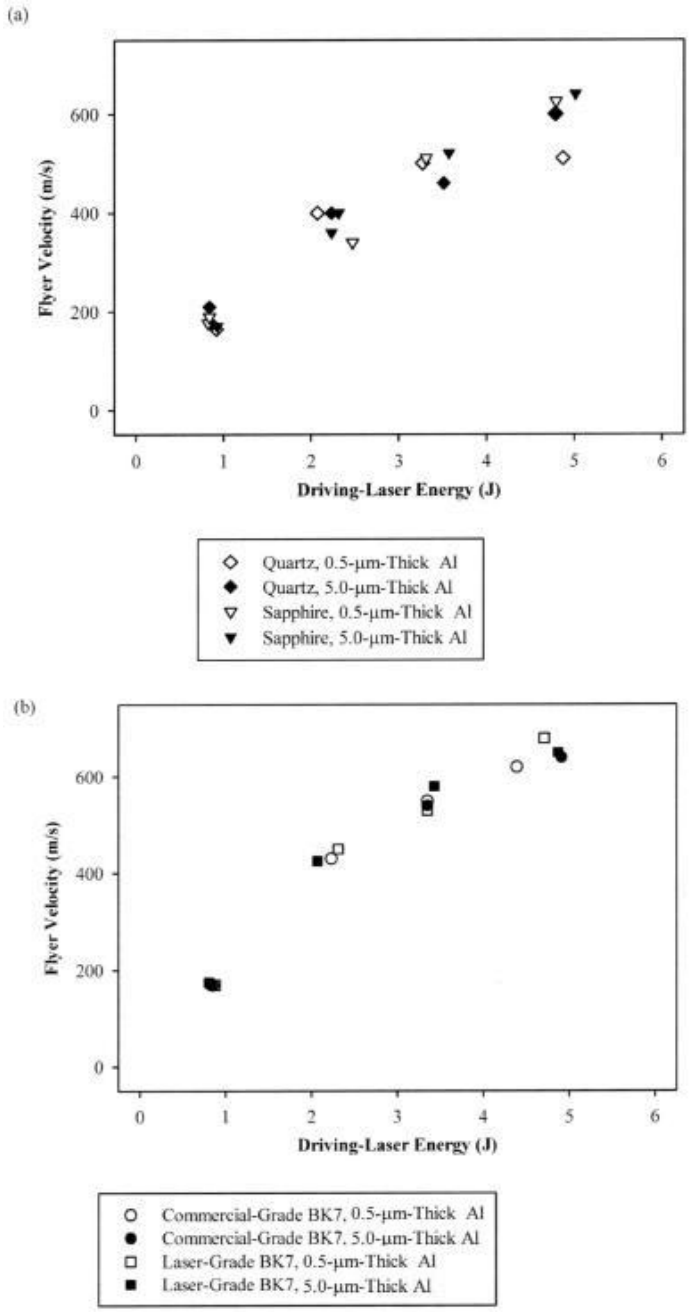

Figure 6: Flyer velocity versus driving-laser pulse energy for (a) quartz and sapphire and (b) commercial-grade and laser-grade BK7 window materials (Robbins, 2004).

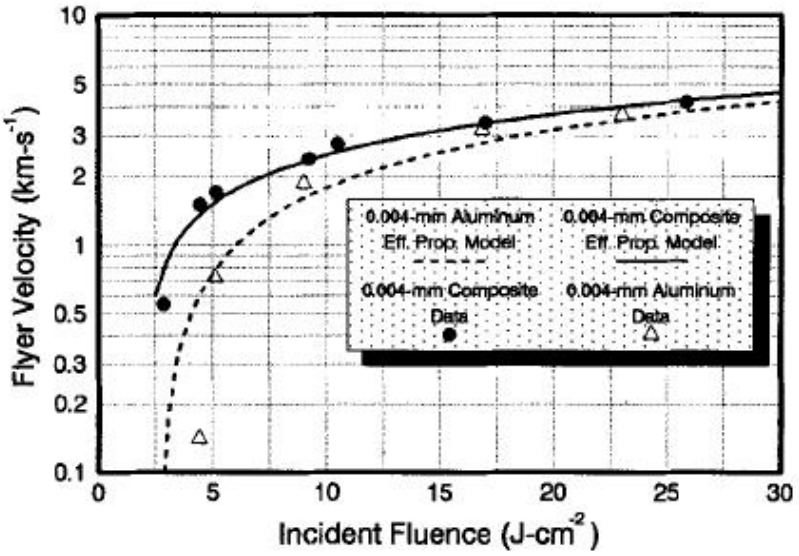

Figure 7: Peak flyer velocities as a function of incident fluence. Comparison of data with analytical model for aluminum and composite targets (Trott, 1994).

were between 3.6 μm- and 4 μm-thick [41, 10]. The velocity results of Trott's performance comparison between aluminum targets and a composite target is shown in Figure 7. Throughout the entire range of incident fluences, the composite flyers attain a higher final velocity for a given driving fluence. The effect is quite pronounced at fluences $< 6\ \frac{J}{cm^2}$ but becomes less pronounced at higher fluences.

The study by Hatt et al. [10] exhibited similar results, as shown in Figure 8. The 3.6 μm-thick multiple layer target achieves approximately 17% higher velocity than the single layer 4 μm-thick Al target after allowing for the difference in the target thicknesses [10]. This result is consistent with Paisley's [23] results showing a $\sim$30% increase in energy conversion efficiency. The efficiency increase can be attributed to the higher shear strength of the aluminum oxide, resulting in a higher pressure before shearing out a metal flyer plate [23].

The studies by Trott [41], Hatt et al. [10], and Paisley [23] also attribute the efficiency increase to the thermal barrier that aluminum oxide provides to buffer the flyer from the radiant exposure of the laser. Robbins et al. [27] state that the aluminum oxide layer also helps to prevent significant flyer heating. Finally, data

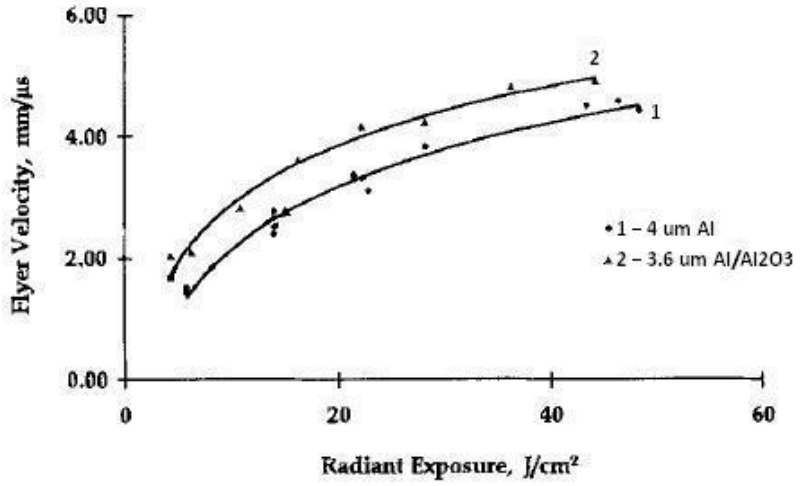

Figure 8: Comparison between various Al targets, showing the effect of a dielectric layer (Hatt, 1996).

from studies by Trott [41] indicate that composite flyers provide better planarity and cohesion of the flyer during flight.

2.3.3 Laser Fluence

The fluence of the driving laser has a significant impact on the final velocity of the flyer, for which the plasma physics driving the flyer requires more study. Ripin et al. [26] considered a rocket analogy to describe the hydrodynamic behavior of the flyer during the acceleration phase. The ablative acceleration uses the thrust of the plasma blow-off on the laser side of the flyer to accelerate the remaining portion of the flyer to high speed. In this model, the plasma was free to expand in any direction, cutting the efficiency of the flyer launch.

The next development in theoretical analysis of laser-driven miniflyers was by Lawrence and Trott [20] in which they used conservation of energy in the framework of the Gurney theory used for acceleration of metal plates with explosives [9]. In order to generate a model that was easy to use and that would describe all major features of the dynamic response of the system, some simplifying assumptions and approximations were made. The most basic was that the energy deposition in the

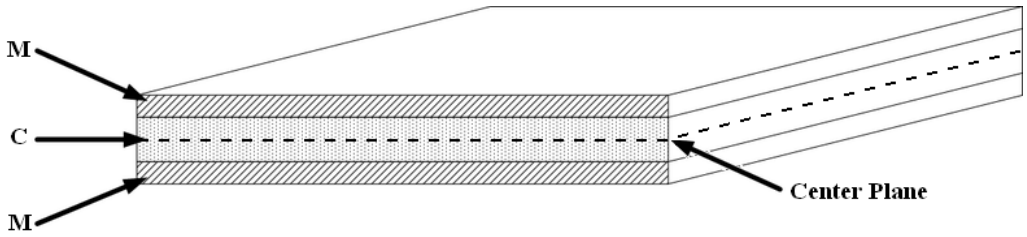

Figure 9: Symmetrical sandwich configuration with center plane comprising of flat explosive layer of mass C and two flyer plates of mass M each, used to study the explosive-metal interaction and resulting acceleration of metal plates.

flyer, the vaporization and blow-off phenomena, and the forces driving the flyer were all one dimensional (i.e. the flyer was thin compared to its lateral dimensions, and the laser fluence was uniform on the substrate). The next assumption was that the substrate is transparent to the driving laser's wavelength, but mechanically rigid with respect to the blow-off products from the flyer. The deposition of the laser energy in the flyer was approximated with a standard exponential profile controlled by an effective absorption coefficient. This coefficient is a function of the laser absorption coefficient and the laser pulse duration. The last approximation was a key part of the Gurney theory [20]. It represents the spatial velocity distribution of the blow-off products as a linear function, extending from zero at the rigid substrate to the actual flyer velocity at the blow-off/solid interface [20].

To apply the Gurney theory, Lawrence and Trott [20] treated the constrained configuration as one-half of a "symmetric sandwich" as described by Kennedy [18] and shown in Figure 9. In the planar geometry, the vaporized portion of the flyer replaced the high explosive of the original theory and the substrate served as the plane of symmetry. This allowed Lawrence and Trott [20] to base their equations on the conservation of energy. Equating the "potential energy" deposited in the flyer by the laser with the kinetic energy of both the blow-off products and the remaining solid portion of the plate yields [20]

$$\rho x_d E = (\rho/2)(x_0 - x_d)v_0^2 + (\rho/2)\int_0^{x_d} (v_0 x/x_d)^2\, dx. \qquad (1)$$

The left hand side of the equation represents the energy available in the blow-off for accelerating the flyer, where ρ is the flyer density, x_d is the thickness of the layer that is vaporized by the laser, and E is the Gurney energy. The first term on the right is the kinetic energy of the flyer, which has an original thickness x_d and a final uniform velocity v_0. The last term on the right is the kinetic energy of the blow-off material. Lawrence and Trott [20] assumed a linear Lagrangian velocity profile of the form [20]

$$v(x) = (v_o/x_d)x, \quad 0 \leq x \leq x_d. \tag{2}$$

Because of the one-dimensional planar geometry, each term in Eq. 1 has units of energy per unit area. This expression can be solved easily for the flyer velocity v_o, obtaining [20]

$$v_o = \sqrt{\frac{3E}{3x_o/2x_d - 1}}. \tag{3}$$

There are no difficulties with this equation unless $x_d \geq 3x_o/2$, an impossible situation since $x_d < x_o$.

To use Eq. 3, definitions must be provided for both the Gurney energy E and the blow-off depth x_d. Lawrence and Trott [20] first assumed that the energy in the laser pulse is deposited exponentially in the flyer according to an effective absorption coefficient, μ_{eff}. Lawrence found that the velocity of the flyer was relatively insensitive to the energy deposition profile [19], so Lambert's Law was used to find the energy per unit mass in the flyer, $\epsilon(x)$ [20]

$$\epsilon(x) = \mu_{eff} F_o (1 - r) \exp(-\mu_{eff} \rho x), \tag{4}$$

where F_o is the laser fluence incident on the flyer, and r is the effective fractional energy loss. Energy can be lost due to reflection and radiation and is integrated over the entire time of interaction. This deposition profile is illustrated in Figure 10, where it is important to note that the energy at the inner surface of the flyer is $\epsilon(x) = \mu_{eff} F_o (1 - r)$.

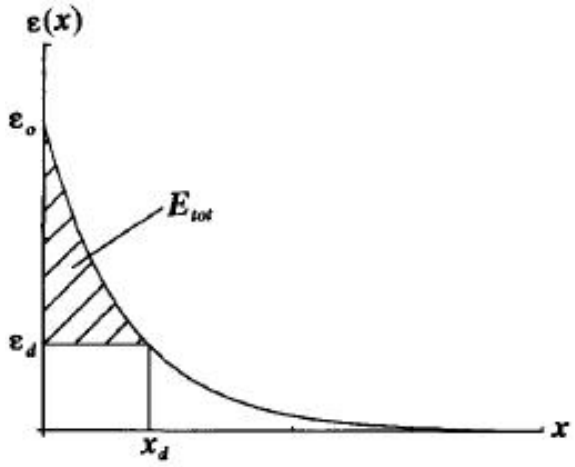

Figure 10: Exponential energy deposition profile (Lawrence, 1993).

Pulse-width dependence was incorporated into the model by taking μ_{eff} to be a function of both the true mass absorption coefficient, μ_α, and the laser pulse duration, τ. The form Lawrence and Trott chose was [20]

$$\mu_{eff} = \frac{\mu_\alpha}{1 + k\mu_a\rho\sqrt{\alpha\tau}}, \tag{5}$$

where α is the thermal diffusivity of the flyer. α is related to common thermal properties through the equation $\alpha = K/\rho c_p$, where K is the thermal conductivity and c_p is the specific heat. Lawrence and Trott [20] added the constant, k, to allow for uncertainties in the handbook values for μ_α and α.

The thickness, x_d, of the layer vaporized from the flyer is determined by finding the depth at which the deposited energy is equal to the vaporization energy, ϵ_d. Lawrence and Trott [20] then solve Eq. 4 in the form $\epsilon(x_d) = \epsilon_d$, obtaining [20]

$$x_d = \frac{1}{\mu_{eff}\rho} \ln\left(\frac{\mu_{eff}F_o(1-r)}{\epsilon_d}\right), \tag{6}$$

as suggested in Figure 10. The amount of energy available for accelerating the flyer, E_{tot} (indicated in Figure 10), is the energy above ϵ_d and contained in the blowoff later. It can be found from [20]

$$E_{tot} = \int_0^{x_d} [\epsilon(x) - \epsilon_d]\, dx, \tag{7}$$

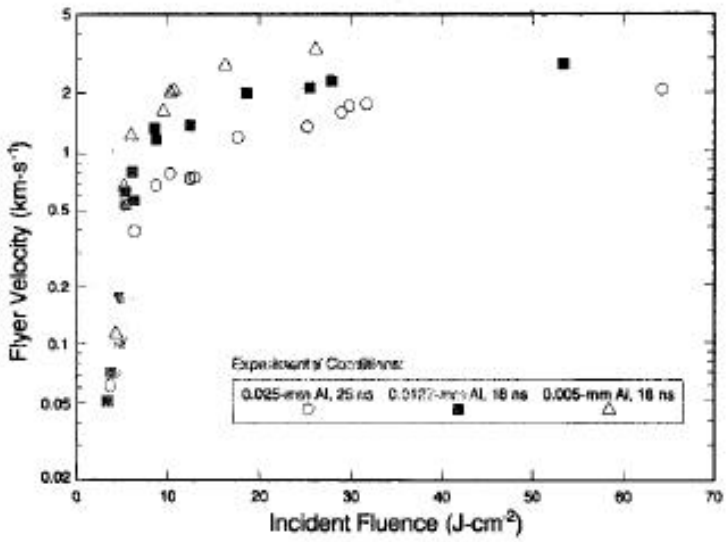

Figure 11: Peak flyer velocities versus incident fluence for indicated foil thicknesses and laser pulse durations (Trott, 1991).

where $\epsilon(x)$ and x_d are obtained from Eq. 4 and 6. This leads to [20]

$$E_{tot} = \frac{F_o(1-r)}{\rho} - \epsilon_d \left(\frac{1}{\mu_{eff}\rho} + x_d \right). \tag{8}$$

The first term on the right is the total deposited energy, and the second term on the right represents the amount that cannot be converted into kinetic energy. This amount arises from energy lost to deposition beyond the blow-off depth, $\epsilon_d/\mu_{eff}\rho$, and energy used for vaporization, $\epsilon_d x_d$. Finally, Lawrence and Trott [20] define the Gurney energy as this latter value, E_{tot}, averaged over the thickness of the blow-off layer, $E = E_{tot}/x_d$, or [20]

$$E = \frac{F_o(1-r)}{\rho x_d} - \epsilon_d \left(1 + \frac{1}{\mu_{eff}\rho x_d} \right). \tag{9}$$

To use the model for predicting flyer velocity, Lawrence and Trott [20] first calculate the effective absorption coefficient, μ_{eff}. from Eq. 5. Then, for each laser fluence of interest, they find x_d from Eq. 6, and E from Eq. 9. The flyer velocity, v_o, follows from Eq. 3.

The results of this derivation are supported by the earlier experimental results of Trott et al. [40, 42] shown in Figures 11 and 12. Both studies have found that the

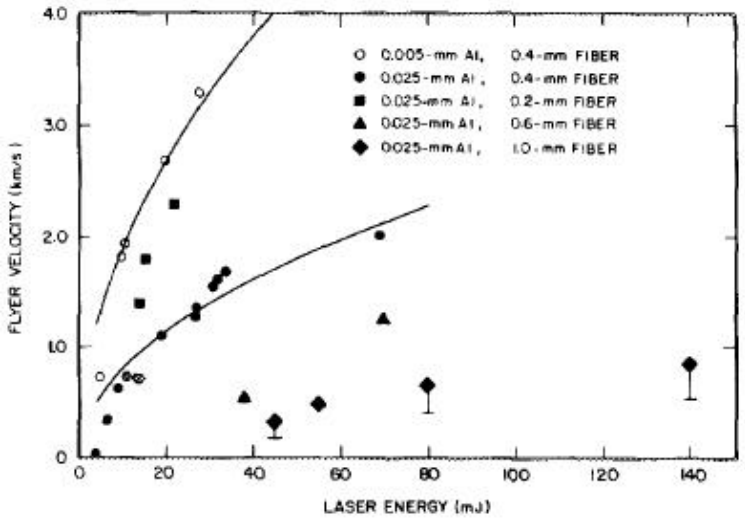

Figure 12: Peak flyer velocities versus laser energy with least squares fits assuming a square root dependence of foil velocity on laser energy (Trott, 1990).

peak flyer velocity scaled with the square root of fluence, suggesting a simple kinetic-energy relationship assuming a small ablated mass fraction and a nearly constant efficiency of coupling optical energy into flyer kinetic energy, k, or [40, 42]

$$v = \sqrt{\frac{2kE}{m}}. \tag{10}$$

Conversion efficiency was found to decrease from fluences $< 10\ \frac{J}{cm^2}$ until fluences of $3\ \frac{J}{cm^2}$ where flyer acceleration did not occur [40, 42].

It is important to note that the above studies were done using fiber-optic coupling techniques. However, Lawrence and Trott [20] considered the case of substrate mounted flyers with lens-coupling and found that because of the different coupling method, the delivery of the laser energy to the flyer was less efficient than with the fiber [20]. An energy loss fraction of $r = 0.78$ was needed to match the data [20]. All other input constants were the same. The results, plotted in Figure 13, show very good agreement between theory and experiment. Changes in laser fluence uniformity across the flyer diameter did not lead to any significant anomalies in the flyer response [20], supporting previous studies by Lawrence [19]. More recently, though, He et al. [11] has observed that at laser intensities higher than $50\ \frac{GW}{cm^2}$, the relationship between

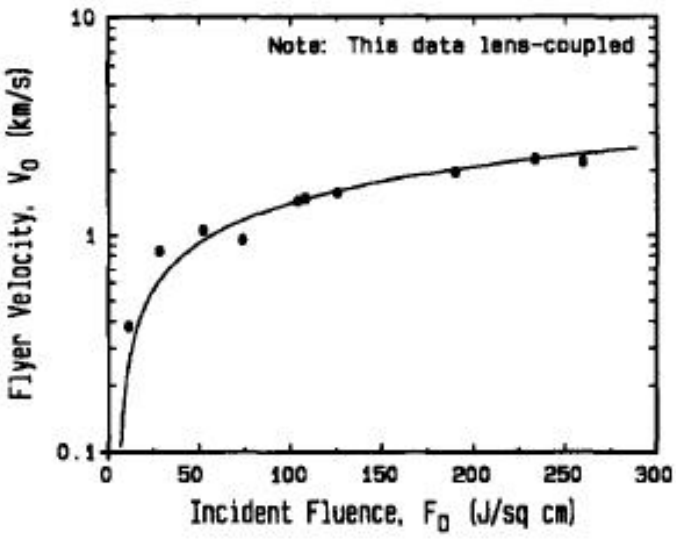

Figure 13: Comparisons between theory and experiment for lens-coupled Al flyers (Lawrence, 1993).

laser fluence and flyer velocity is more complex and cannot be explained by a simple kinetic-energy relationship.

2.3.4 Drive Laser Characteristics

One of the requirements for the laser-driven miniflyer system is a laser beam with a uniform cross-section. For uniform irradiance of the flyer, it is desirable that the Gaussian profile of the Nd:YAG laser is transformed into a flat-top profile. Beam shaping is the process of redistributing the irradiance and phase of a beam of optical radiation [7]. The beam shape is defined by the irradiance distribution and the phase of the shaped beam. The output of the shaping optic is a collimated beam with a prescribed radial profile that is nearly constant over a substantial range of propagation [13]. Laser beam shaping techniques can be divided into three broad classes. The first is the use of an aperture to select a suitably flat portion of a beam, illustrated in Figure 14. The main disadvantage of this method is that the technique is not loss-less. For the laser-driven miniflyer system, laser energy losses are undesirable.

The second major technique for beam shaping is field mapping, in which the

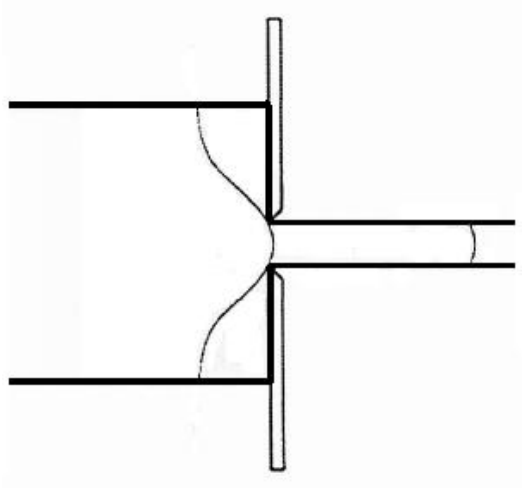

Figure 14: Uniform irradiance obtained by aperturing input beam (Dickey, 2000).

amplitude and phase of the incident beam is transformed in a deterministic fashion defined by the shape of the refractive surfaces [13]. This method can be effectively loss-less and works well for single-mode beams of known profile [30]. The remaining technique is beam integration. A beam integrator breaks the input beam into a large number of facets by a lens-array, then tries to spread the energy within each facet over the output region [30]. The output beam profile is a sum of the diffraction patterns of each lens-array aperture [30]. Beam integrators are suited for multi-mode beams where the input profile may be unknown.

The laser-driven miniflyer system using a single-mode beam of known profile requires field mapping as the best option for beam shaping. The basic field mapping layout is shown in Figure 15. For both setups the first aspheric surface redistributes rays in such a way as to transform the profile and the second aspheric surface recollimates the beam. To avoid internal focus that can limit power handling capabilities as in the Keplerian geometry, a Galilean geometry is best for the laser-driven miniflyer system.

A Gaussian to flat-top beam transformation must satisfy several requirements: uniformity of the output beam, efficient utilization of the input beam power, and

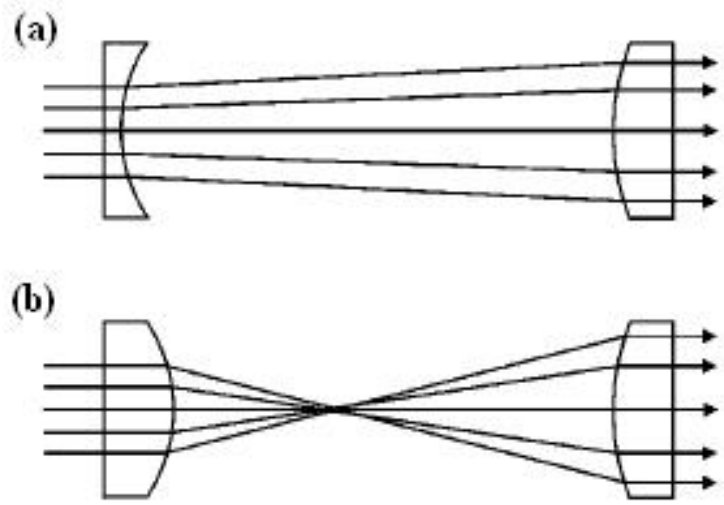

Figure 15: Schematic layout of two-lens beam reshaping optics illustrating the (a) Galilean and (b) Keplerian geometries (Hoffnagle, 2003).

propagation of the beam across a useful range [13]. To best quantify this transformation, calculating the parameter β helps to determine the quality of the transformation [30]

$$\beta = \frac{2\sqrt{2\pi} r_o Y_o}{f\lambda}, \tag{11}$$

where λ is the wavelength, r_o is the beam radius, Y_o is the half-width of the desired output dimensions, and f is the focal length of the focusing optic, or the working distance from the optical system to the target plane. For simple geometries, the following guidelines apply:

- If β <4, a beam shaping system will not produce acceptable results.
- When 4< β <32, diffraction effects are significant and should be a part of the design of the beam shaping system.
- When β >32, geometrical methods should be adequate for design of beam shaping systems.

Figure 16 shows how changes in β affect the final shape of the flat-top beam.

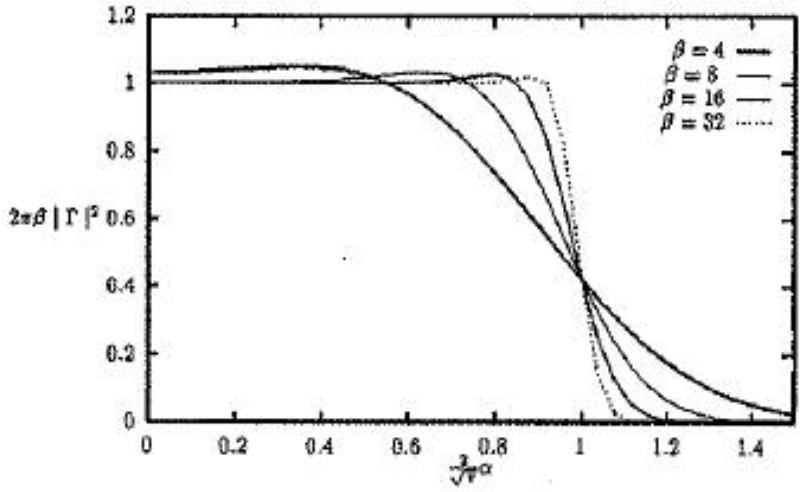

Figure 16: Beam intensity variations with changes in β (Romero, 1996).

The shape of the incident laser beam can affect the planarity of flight of the flyer. Watson and Field [43] stated that better integrity of the flyers can be expected if the flyers are launched with a top-hat beam profile. A more 1-D ablation profile would be produced leading to a more planar flyer profile and reduced shear forces within the flyer which can cause break-up of the flyer [43].

2.4 Velocity Measurement Diagnostics

Velocimetry is one of the primary diagnostic tools used in shock physics experiments. Laser velocimetry is one of the few ways to get accurate velocity results with laser-driven miniflyer system experiments due to the small scale of the target and the short flight path. One of the diagnostics that works well with the miniflyer system is Photonic Doppler Velocimetry (PDV). This system is based on the Doppler effect, a shift in frequency and wavelength of waves which results from a source moving with respect to a medium. The velocimetry system creates and analyzes the beat pattern that occurs when the unshifted light is combined with the shifted light in a different way. Figure 17 shows how two high frequency waves combine to create a beat pattern.

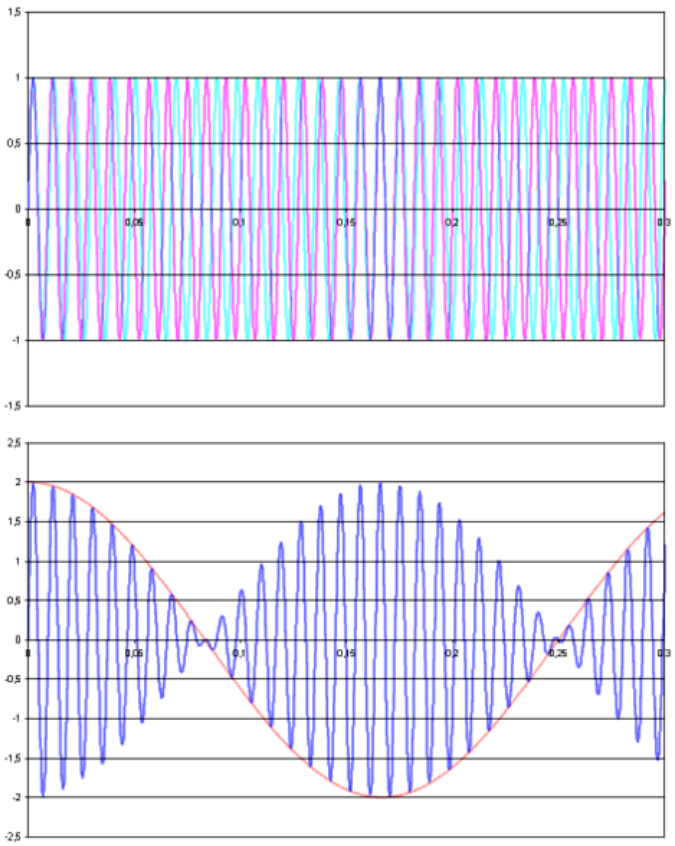

Figure 17: A 110 Hz sine wave (cyan) beating with a 104 Hz sine wave (magenta) to create a beat frequency of 6 Hz (red).

Table 1: PDV primary components and vendors (Strand, 2005).

Component	Vendor	Model Number or Type
Fiber Laser	IPG Photonics	ELD-2-1550-SE
Circulator	JDS Uniphase	CIR-230031000
Single mode fiber	Corning	SMF-28
Probe	Oz Optics	Various
Detector	Newport Corporation	AD-70xr-FC
Amplifier	Picosecond Labs	5840A
Digitizer	Agilent Technologies	54885A Infinium

2.4.1 Photonic Doppler Velocimeter

PDV is a new development in velocimetry made possible by the telecommunication industry's commercialization of high bandwidth electrical components that utilize single-mode fiber-optics operating at 1550 nm [35]. Table 1 contains a list of the primary components and their vendors used to create a typical PDV system such as the one at Lawrence Livermore National Laboratory [35]. All items are commercially available and relatively low-cost, making the creation of a PDV system more accessible.

The basic geometry of a PDV is shown in Figure 18. A single-mode 1550 nm laser is used to illuminate the moving surface to be measured. Optical fibers are used to transport light from the laser to a probe containing a focusing lens. This same probe then collects light that is scattered or reflected from the moving surface and sends the Doppler-shifted light to the detector. Non-shifted light is also routed straight from the input laser to the detector. The beat signal is generated at the detector by mixing the shifted and non-shifted light signals. The frequency of the light emitted by the laser is $f_o = \frac{c}{\lambda}$ where c is the speed of light and the frequency of the Doppler-shifted light is $f_d(t)$. The beat signal is generated at the detector with a frequency $f_b(t)$ equal to the absolute value of the difference between the Doppler-shifted frequency and the non-shifted frequency $f_b(t) = |f_d(t) - f_o|$. The beat frequency $f_b(t)$ is then related to

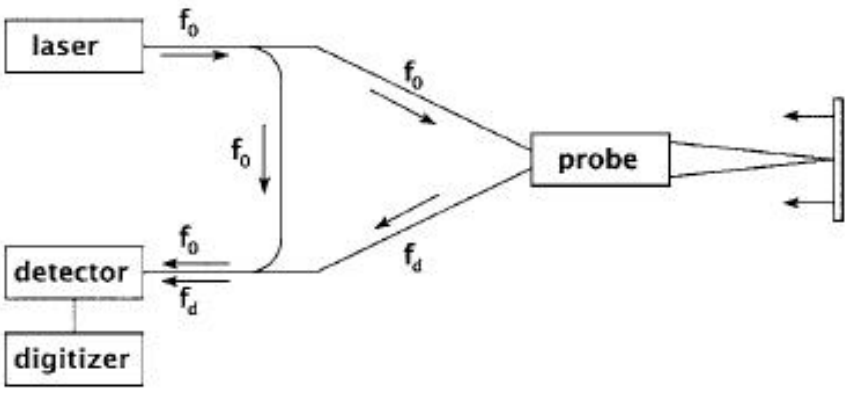

Figure 18: The basic geometry of a PDV system (Strand, 2006).

the velocity $v(t)$ by [34]

$$f_b(t) = |f_d(t) - f_o| = 2\left[\frac{v(t)}{c}\right] f_o. \tag{12}$$

In nearly all of the experiments at Lawrence Livermore National Laboratory the Doppler-shifted light is greater than the original laser frequency, that is, $f_d(t) > f_o$ [34]. Because the PDV system responds to the absolute value of the beat frequency, it cannot tell the difference between a surface moving toward the probe or a surface moving away from the probe with the same speed [34].

The heart of the PDV design is based on a fiber-optic component called a three-port circulator (Figure 19) [35, 34]. The circulator has the property that light injected into port 1 will be emitted out of port 2, but not port 3. Light injected into port 2 will be emitted out of port 3, but not port 1. The efficiency for the transportation from port 1 to port 2 and from port 2 to port 3 is 0.85 while the efficiency for transporting light in any other direction is $< 10^{-6}$ [34]. The fiber laser is connected onto port 1, the probe onto port 2, and the detector system onto port 3. Since the entire system is fiber-coupled, efficiency is quite high overall [34]. The source of non-Doppler-shifted light comes from the fiber end face of the probe in the setup at LLNL because non-shifted light cannot travel from port 1 to port 3 directly [34]. In the PDV system at the High Strain Rate Lab at Georgia Tech, the non-shifted light comes from a

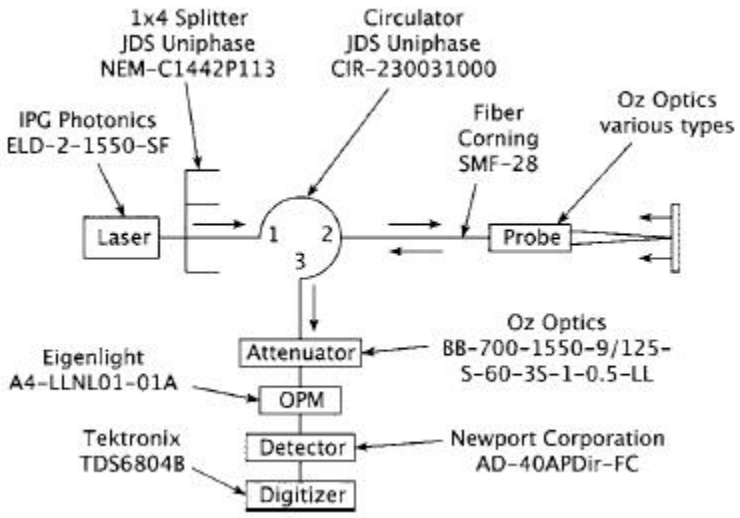

Figure 19: The PDV system shown with three-port circulator, component vendors, and parts numbers (Strand, 2006).

retroreflector split off from the fiber-optic feed to the probe. This allows the amount of unshifted light to be adjusted for the power optimization at the detector.

The new digitizers that have come to market have very high bandwidths, very high sample rates, and large amounts of memory. Strand et al. [34] use a Tektronix digitizer with an 8 GHz bandwidth, sample rate of 20 $\frac{GS}{S}$ per channel, and enough memory to record for 1.6 ms. The Nyquist limit for recording a wave form is equal to one-half the sample rate, which means that a 10 GHz beat wave form could, in theory, be recorded and the frequency determined [34]. A beat signal with that frequency would correspond to a velocity of 7750 $\frac{m}{s}$. The maximum velocity is also limited by the bandwidth of the system. The detectors at LLNL have 12 GHz bandwidth, which when coupled with 8 GHz bandwidth of the digitizer give

$$BW = \frac{0.35}{t_r}, \quad \text{where } t_r \text{ is rise time} \tag{13}$$

$$t^2_{r,system} = t^2_{r,1} + t^2_{r,2} + \dots \tag{14}$$

yielding a total bandwidth of ~ 6.7 GHz and a maximum velocity of 5160 $\frac{m}{s}$ [34].

PDV data analysis is done using a sliding Fourier transform method [34]. Laser

wavelength, time per point in the data record, and the desired number of points in the Fourier transform window are input in the analysis software. The sliding Fourier transform algorithm calculates the frequency spectrum for the first temporal window, then advances a specified amount of time and calculates the next frequency spectrum. Strand et al. [34] tested the Fourier transform on 100% random noise and found an average velocity error of only 0.01%, but after more testing found a velocity uncertainty of $\sim 1\%$ to be more realistic.

There are many advantages to the PDV system. It is an all-fiber system that only requires contrast adjustment [17]. The tracking distance, i.e. the length over which useful data is returned, can track up to 15 mm [17]. The PDV system itself is compact and relatively inexpensive [34], as well as being efficient due to fiber coupling. Fluctuations in light intensity can be seen in the data, but the PDV system is robust against large variations [34]. Because the PDV system creates a beat frequency based off of the original laser frequency, velocity measurements are based on a constant baseline. This means that a drop in data does not affect analysis of the rest of the signals. Analyzing the data using Fourier transform techniques allows observation of multiple discrete velocities, as well as dispersion [34]. The disadvantages of PDV include a large dynamic range requirement to continue measurement with extreme low or high beat amplitudes [35]. Also, acoustic modes in the fibers can introduce noise [17]. Temporal resolution is limited to 10 ns, which can make measurement of shock break-out more difficult [17].

CHAPTER III

LASER-DRIVEN MINIFLYER SET-UP: LAYOUT AND COMPONENTS

The setup of the miniflyer system in the High Strain Rate Lab at Georgia Tech consists of three parts. The first part is the drive laser, a Continuum Powerlite Precision II Plus operated at 1064 nm and injection seeded to improve beam quality. The 12 mm-diameter beam first travels through a Faraday isolator to ensure no reflected light reenters the laser. Mirrors then redirect the beam through an 8 mm aperture that cuts off the outer 2 mm of the Gaussian beam (Figure 20) or a refractive beam shaper (Figure 21). The refractive beam shaper is preceded by a lens pair to focus the 12 mm-diameter beam down to the 5 mm-diameter needed to enter the beam shaper. A 250 mm focusing lens focuses the beam on to the substrate/flyer assembly; the second part of the miniflyer system. The size of the irradiant area can be adjusted by moving the focus lens closer or farther away from the substrate/flyer assembly. The energy of the laser is absorbed by the composite coating layer deposited on to the substrate. A plasma is created from this energy absorption. As the plasma expands, the flyer is accelerated with a velocity related to the energy of the pulse and the mass of the flyer. PDV diagnostics constitute the third part of the miniflyer system, and are used to measure the velocity of the flyer plate. Detail of the components and the layout of each part is described next.

This chapter is divided into three sections: laser drive source, impact experiment assembly, and time-resolved diagnostics. The laser drive source section includes everything used to create the final pulse that impacts the substrate on to which the miniflyer is attached. The impact experiment assembly is the chamber and everything

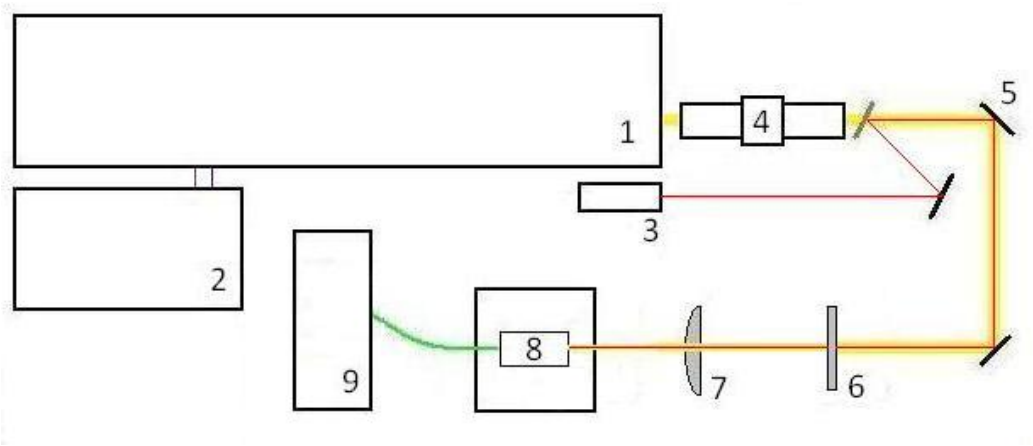

Figure 20: Miniflyer system table layout 1: (1) 3 J Nd:YAG 1064 nm driving laser, (2) fiber optic coupled injection seeder laser, (3) 2.7 mW Diode 635 nm alignment laser, (4) Faraday isolator, (5) high-energy mirrors, (6) 8 mm aperture, (7) 250 mm focusing lens, (8) experiment chamber, (9) laser diagnostics.

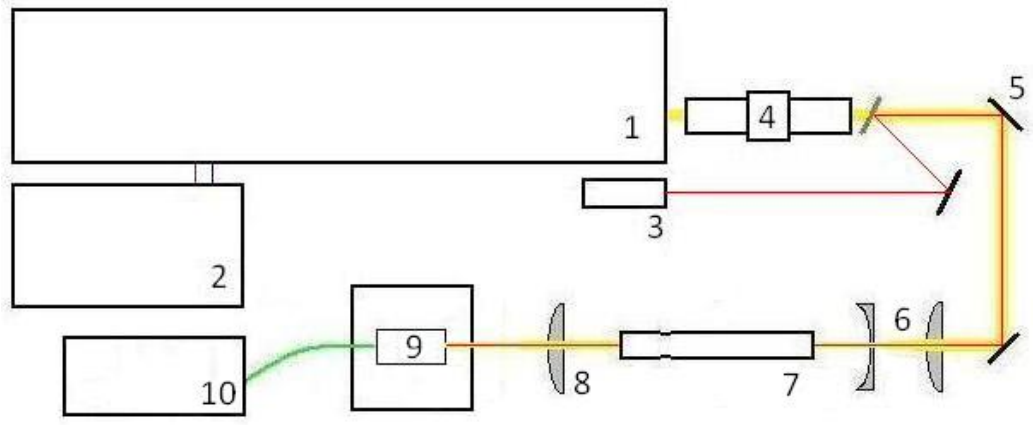

Figure 21: Miniflyer system table layout 2: (1) 3 J Nd:YAG 1064 nm driving laser, (2) fiber optic coupled injection seeder laser, (3) 2.7 mW Diode 635 nm alignment laser, (4) Faraday isolator, (5) high-energy mirrors, (6) beam resizing optics, (7) refractive beam shaper, (8) 250 mm focusing lens, (9) experiment chamber, (10) laser diagnostics.

within it. Time-resolved diagnostics includes all equipment used to characterize the flight of the flyer and measure the particle velocity at the rear surface of the specimen.

3.1 Laser Drive Source

The first part of the laser-driven miniflyer system directs a spatially-shaped pulse of desired amplitude and uniformity onto the substrate/flyer assembly. The characteristics and components are described below.

3.1.1 Drive Laser Characteristics

The driving laser used to launch the flyer is a Q-switched Nd:YAG laser consisting of an oscillator and two amplifiers. The oscillator produces a single 10 ns pulse with a maximum pulse energy of 3 J. The output beam has a diameter of 12 mm. Upon exiting the laser, the beam travels through a Faraday isolator made by Electro-Optics technology. The Faraday isolator prevents any stray reflected beams from re-entering the laser cavity and causing damage to the laser. At lower laser power, the isolator transmits $\sim 90\%$ of the laser energy, but at higher laser power, the isolator transmits $\sim 80\%$ of the laser energy. Two high-energy Nd:YAG laser mirrors made of UV grade fused silica substrates and ultrahard dielectric coatings are used to steer the beam toward the target chamber. An 8 mm aperture is used to sample a portion of the Gaussian beam. The aperture also introduces a diffraction pattern on the beam profile. Figure 22 shows the Gaussian beam profile before the experiment chamber without the apertrue in place and Figure 23 shows the psuedo-top hat beam profile before the experiment chamber with the aperature in place.

Figure 24 shows the beam profile after passing through a refractive beam shaper. The flat-top beam profile from the beam shaper is not significantly improved over the beam profile created by use of the aperture. The beam shaper has a damage threshold of 10 $\frac{J}{cm^2}$ peak energy, this limits the input beam energy to 981 mJ. After a 10% loss from the beam shaper, the maximum laser fluence that can be used to

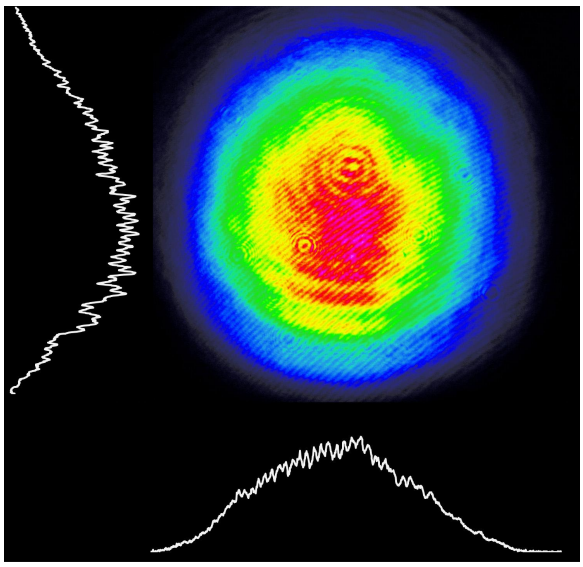

Figure 22: Gaussian beam profile of the driving laser.

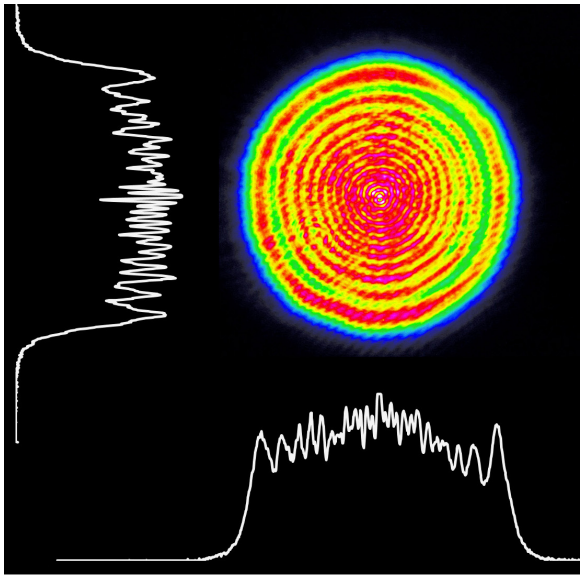

Figure 23: Psuedo-top hat profile created by the 8 mm aperture.

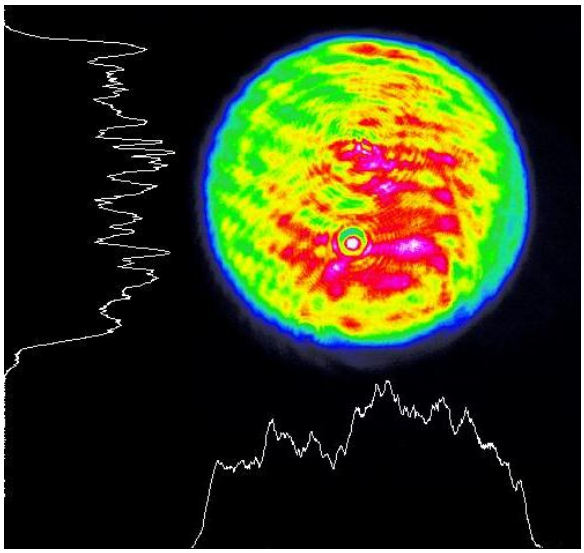

Figure 24: Psuedo-top hat profile created by the refractive beam shaper.

launch a flyer is 900 mJ. The aperture has a transmittance of 45%, so at maximum drive laser output of 3 J only 1350 mJ is available to drive the miniflyer. Given that the flat top profile created by the beam shaper is not significantly different from that of the aperture, the 8 mm aperture is used to shape the beam because it allows higher fluences to be used.

3.1.2 Laser-Drive Source Components

3.1.2.1 Nd:YAG Laser

The Continuum Powerlite Precision II Plus is used for its high power and beam quality. The Gaussian mirror coupled resonator is optimally mode-filled for maximum energy extraction allowing amplification up to 3 J per pulse [6]. Within thirty minutes, the laser has a pointing stability of $<\pm 30$ μrad and divergence of 0.45 mrad. The far-field beam has a nearly Gaussian profile with a least squares fit of 0.95 (a coefficient of 1 would be perfect). During use, the laser uses 1-3 gallons of city water per minute to maintain the power supply around 88°F.

3.1.2.2 Seeder Laser

The seeder laser is a Continuum Surelite I-10. Its purpose is to produce an ultra-narrow Single Longitudinal Mode (SLM) output with a smooth temporal profile [36]. This SLM output is used to control the properties of the high power oscillator in the Powerlite. A seed beam is produced by injecting a beam from a single mode continuous-wave diode fiber laser into the resonator of the Surelite oscillator. The resulting beam is injected into the Powerlite oscillator and serves as a seed from which the pulsed laser output grows [4]. The reason for this is that the spectral properties of a low power laser are much easier to control than those of a high powered laser. The seeder laser is able to produce an SLM output at 1064 nm from which the Powerlite can base its output. This works by the fact that naturally occurring pulses always begin from a zero point energy of the laser resonator or from spontaneous emission. If the injected seed is large enough, the pulse growing from the injected seed will overwhelm the naturally occurring pulse in the high power laser. When this happens, the laser output mimics the properties of the seed rather than its own properties. In this way, the Powerlite Precision II Plus is able to emit up to 3 J while still maintaining the spectral properties of a lower power output laser.

3.1.2.3 Alignment Laser

The alignment laser is a 635 nm diode laser. This visible light laser is used to ensure proper alignment of the laser table setup before the high power laser is sent through the optics. It is important for a user of the miniflyer system to know where the high power beam is. The Powerlite laser operates at 1064 nm, which is in the infrared part of the spectrum, thus light emitted by the laser is invisible to the human eye. The high power beam can cause serious burns and/or blindness, so it is important to know where it is at all times. The visible alignment beam allows the user to check for stray reflections and any other issues that may be a problem when the Nd:YAG

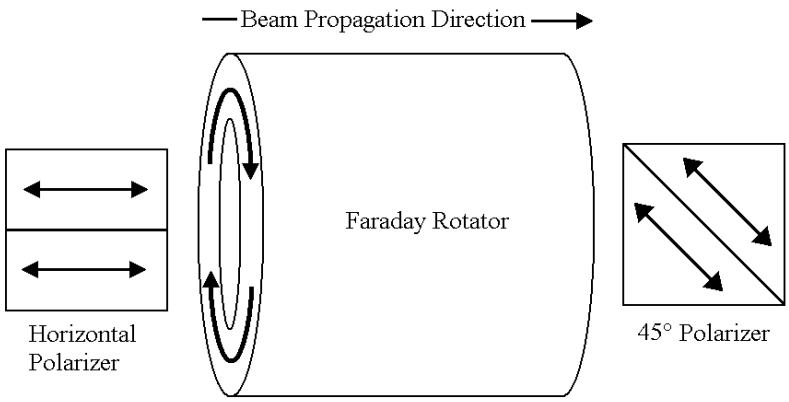

Figure 25: The three components of a Faraday isolator (light traveling left to right). Light travels through easily.

laser is on full power. Once the system is set up and locked in, the alignment laser is only used when changes to the table layout are made and for aligning experiments.

3.1.2.4 Faraday Isolator

The Faraday isolator made by Electro-Optics Technology is used in our miniflyer acceleration system. It functions as a one-way light valve, permitting radiation to pass through in only one direction and not the other, thus preventing harmful back-reflections from reaching the laser source [22]. The Powerlite laser emits light that is horizontally, linearly polarized. The horizontally polarized light travels freely through the input polarizer. As the light travels from left to right through the Faraday rotator it is rotated 45° clockwise. It exits through the 45° polarized output polarizer. If any light were to reflect back into the Faraday isolator it would enter through the output polarizer at 45°, rotate 45° more in the Faraday rotator, and then hit the input polarizer vertically polarized. Since vertically polarized light can not travel through a horizontal polarizer, the reflected beam is effectively blocked. Figures 25 and 26 show the process by which a Faraday isolator works.

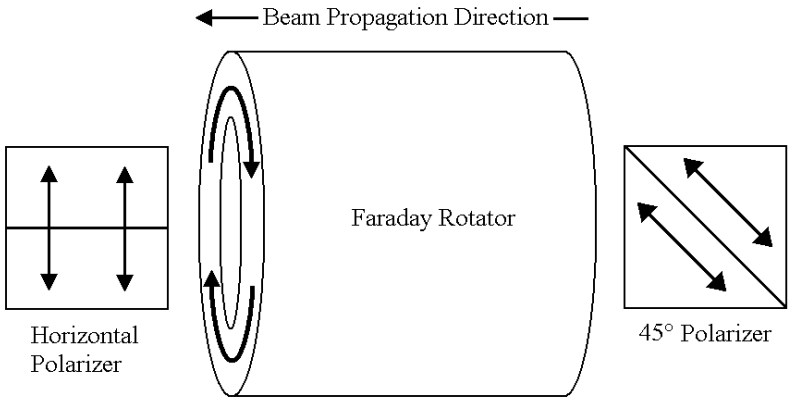

Figure 26: The three components of a Faraday isolator (light traveling right to left). Light is blocked by the input polarizer.

3.1.2.5 High-Energy Mirrors

The high-energy Nd:YAG laser mirrors used in the laser-driven miniflyer system are made of UV grade fused silica substrates and ultra-hard dielectric coatings. They are designed to withstand high-energy pulses and have a high damage threshold. This is very important as the Powerlite laser emits 3 J over a circle with a diameter of 12 mm. This gives the laser a fluence of 2.65 $\frac{J}{cm^2}$ at its original beam size. When the beam is focused to its final size of 3 mm in diameter, the fluence becomes 42.44 $\frac{J}{cm^2}$. The turning mirrors used in the system will withstand fluences of 10 $\frac{J}{cm^2}$ at 1064 nm, so in order to prevent damage, the minimum diameter of the beam when hitting a turning mirror must be 6.2 mm.

3.1.2.6 Optics

The optics in the system are used to size the laser beam to fit the 5 mm diameter input of the beam shaper before bringing the final beam diameter to 3 mm. As with the mirrors, it is important that these optics are designed to withstand high fluences. They must also have an anti-reflective (AR) coating to prevent light from traveling back through the system. The spherical lenses used are made of the same UV grade fused silica as the mirrors and have a damage threshold of 3 $\frac{J}{cm^2}$. They have a $\lambda/8$

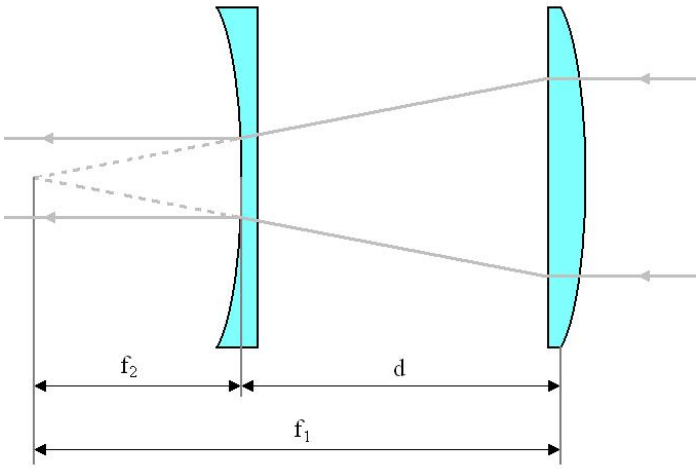

Figure 27: The effects of lenses on the beam size.

surface irregularity and 20-10 scratch-dig, as well as the AR.33 laser line multilayer V-coating that gives a $R_{max} < 0.25\%$ at 1064 nm. The plano convex lenses have a focal length of 250 mm, and the plano concave lens has a focal length of -100 mm. Figure 27 shows the effect the lenses have on the beam size as it travels through the optics, as well as the distances needed to produce these effects.

By using the same setup as a beam expander, but reversing the direction of light, the laser beam can be condensed to a smaller diameter. The inverse equation of magnification is used to determine the ratio that the beam diameter is condensed.

$$\text{Magnification}^{-1} = \frac{f_2}{f_1}$$

The distance between lenses is determined by the equation $d = f_1 - \mid f_2 \mid$. Using the equations above, it is found that the beam diameter will be reduced from 12 mm to 4.8 mm, and the distance between the lenses should be 150 mm.

3.1.2.7 Refractive Beam Shaper

The refractive beam shaper is from Newport optics (GBS-NIR-H3). It is designed for use with high power lasers of wavelength 800-1120nm. Using the parameter β discussed in Chapter 2 can help determine the quality of the transformation from

Gaussian to flat-top

$$\beta = \frac{2\sqrt{2\pi}r_0 Y_0}{f\lambda} \tag{15}$$

where λ is $1.064 * 10^{-3}$ mm, r_0 is 2.5 mm, Y_0 is 4.0 mm, and f is 1000 mm yields a resulting β of 47. Using the following guidelines;

- if β <4, a beam shaping system will not produce acceptable results,
- when 4< β <32, diffraction effects are significant and should be a part of the design of the beam shaping system,
- when β >32, geometrical methods should be adequate for design of beam shaping systems,

it is clear that the beam shaper used for this system is more than adequate for creating a flat-top profile.

It is important to consider the power densities that will be used with the beam shaper as it has a damage threshold of 10 $\frac{J}{cm^2}$. The Gaussian shape output of the Powerlite laser requires the energy density to be multiplied by a factor of two to account for the difference between the peak laser energy and the full-width half-max (FWHM) energy. Figure 28 shows the relation between the FWHM energy and the peak energy. Thus, when doing calculations before a laser shot, a multiplication factor of two should be considered because energy density is calculated using FWHM when using the simple calculation of (laser energy)/(area of laser spot). The beam shaper takes a 5 mm-diameter (at its base) Gaussian input beam and emits an 8 mm-diameter top hat beam. The beam shaper has a transmittance of roughly 90%.

3.1.2.8 Beam Splitter

A pellicle beam splitter can be used to sample $\sim$ 8% of the beam right before the impact experiment assembly. The split-off light can be directed into a beam profiler for analysis of the beam's profile or it can be sent to a power meter for calculations

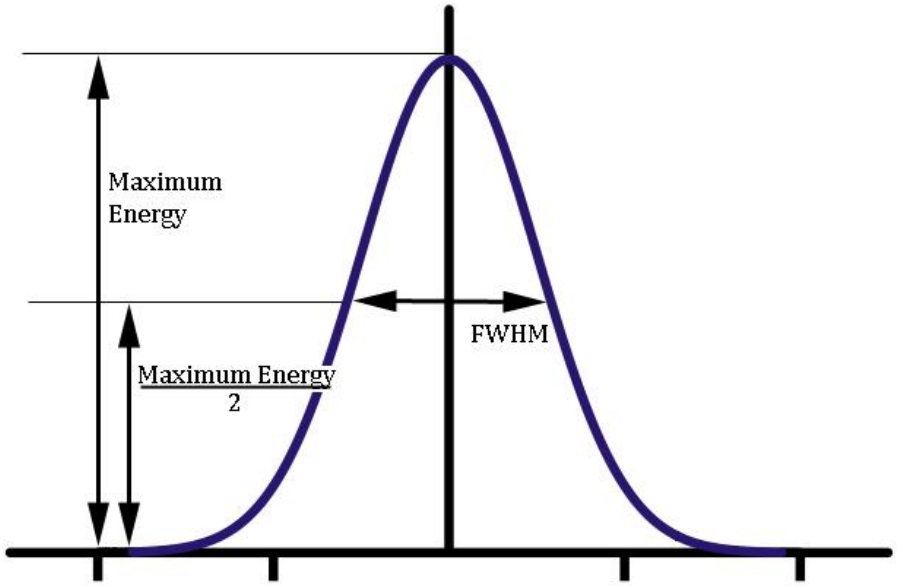

Figure 28: Maximum laser energy versus FWHM laser energy.

of actual beam power hitting the target. There are a couple disadvantages to this method. Through testing, it was found that the beam splitter split-off between 7% and 10% of the laser beam light. Because of this unknown, the decision was made that taking an average of beam power directly from the main laser beam was a more accurate way to predict the power that irradiated the target. The beam profile was found to be quite consistent once the laser-driven miniflyer system was aligned correctly, so the loss of power to split the beam to observe its profile was unnecessary. The beam splitter may be useful in some situations, but the current setup does not use it as a permanent part of the laser system in order to use the largest laser fluence possible for experiments.

3.1.2.9 Beam Profiler

The beam profiler is a Coherent LaserCam-HR featuring a USB 2.0 interface that provides power to the system as well. The LaserCam is able to operate with both continuous-wave and pulsed lasers up to 800 $\frac{mW}{cm^2}$ with the low distortion faceplate attached. The beam profiling system uses PC software that can measure centroid

and peak locations, pointing stability beam width/diameter, divergence, Gaussian fit analysis, elliptical analysis and uniformity analysis. The uniformity analysis is utilized by the High Strain Rate Lab to determine the quality of the flat-top beam after it has been shaped by the beam shaper.

3.1.2.10 Power Meter

The power meter is made by Ophir Laser Measurement Group. The 30(150)A-HE-DIF thermal head is recommended for use with highly concentrated beam Q-switched lasers and it comes with a diffuser head to spread out concentrated beams. The aperture is 17 mm, which is big enough for measurements from any position in the laser system. The maximum energy density for < 100 ns pulses and 10-50 Hz repetition rates is 5 $\frac{J}{cm^2}$ for 1064 nm with the diffuser attached. Without the diffuser attached, the maximum energy density is only 2 $\frac{J}{cm^2}$.

The thermal head is connected to the NOVA II Power Meter. The NOVA II can measure power or energy from pJ and pW to hundreds of Joules and thousands of Watts. The power meter can be connected to a computer as well. Because the Powerlite is a pulsed laser, its energy can change from shot to shot. The software included in the power meter system allows average power or energy to be recorded for a specific number of pulses. This feature is useful in determining the laser fluence at the target when the power meter is included in the beam path.

3.2 Substrate/Flyer Assembly

3.2.1 Window Material

The window material used for the laser-driven miniflyer acceleration experiments is commercial-grade BK7 (ESCO Products). This material is transparent to the driving-laser wavelength just like sapphire, fused silica, and laser-grade BK7, but at half the price of the next cheapest option. Robbins et al. [27] found that BK7 windows yielded slightly higher velocities than the other windows. Laser-grade BK7 yielded slightly

higher velocities overall than commercial-grade BK7, but with a price more than four times that of commercial-grade BK7. Hence, the choice was made to use the low cost option of commercial-grade BK7. All subsequent work is performed using this window material.

3.2.2 Substrate Window Coatings

Flyer plates are mounted on 1.59 mm thick BK7 substrates (ESCO Products) that are coated with a thin film composite of carbon, aluminum oxide and aluminum by Spectrum Thin Films. The first coating on the substrate is a 0.5 μm-thick layer of carbon followed by a 0.5 μm-thick layer of aluminum oxide. The final coating is a 1.5 μm-thick layer of aluminum. The carbon layer acts as a laser light absorber, thus creating a rapidly expanding plasma. The aluminum oxide acts as a thermal barrier between the plasma and the flyer plate, and the aluminum layer helps to contain the plasma to create a more efficient launch of the flyer.

3.2.3 Flyer Material and Thickness

Copper foils of 25 μm-, 50 μm- and 100 μm-thickness are used as the miniflyers. The flyers are cut from the foil sheets using a commercially available metal punch set. Each punch had a starter point that was removed by putting the punches on the lapping wheel for approximately an hour. The 1/8 inch punch cuts a flyer of approximately 3.2 mm-diameter while the 3/32 inch punch cuts a flyer of approximately 2.4 mm-diameter. The flyer disc is typically bent after it is punched out, so it is flattened by rolling an aluminum cylinder on top of it and then pressing it at 10000 pounds between two lapped hardened-steel platens with the hydraulic press. The pressing process also removes any kerf on the flyer edges that may affect the planarity of the flight.

Loctite HYSOL RE2038/HD3475 Electronic Formulated Liquid, a low viscosity, general casting system with excellent electrical and physical properties, is used to

mount the flyer to the coated side of the substrate. Because of the very low viscosity, a very thin bond on the order of a couple of microns can be achieved between the flyer and the outer aluminum coating of the substrate. The epoxy is mixed and put under vacuum for 5-10 minutes to minimize air bubbles. A push pin is used to place a very small drop of epoxy on the substrate. The flyer is then placed on the epoxy drop and the whole assembly is placed between two pieces of Teflon on a granite block. Approximately 15 pounds of dead weight is put on the assembly with a lapped piece of steel between the weight and the assembly to ensure even glue thickness. The epoxy is then allowed to cure for 24 hours. Once the epoxy has cured, the substrate is marked on the uncoated side with a permanent marker to indicate the position of the flyer. An apparatus was created to ensure that the marker spot is directly opposite of the flyer location. This apparatus is pictured in Figure 29. The marker is aligned with the small point of plastic on the bottom so that when the flyer is centered on the plastic point, the marker will mark this position on the other side of the substrate. This positioning is important so that the laser irradiates evenly over the entire flyer area allowing for planar flight of the flyer.

3.2.4 Substrate/Flyer Holder

To allow for multiple shots from one substrate, a substrate/flyer holder was fabricated from PMMA (Figure 30). The substrate/flyer holder has a 19 mm hole that the coated substrate can be mounted in. Lapped spacers are used to maintain consistent distances within the holder. On the back of the substrate/flyer holder is a mount to hold a small piece of acrylic sheet. The acrylic sheet ensures that no flyer debris contacts the PDV probe. It is mounted at an angle to minimize the reflection of the PDV laser. The substrate/flyer holder is mounted on a movable stage so that it can be moved both vertically and horizontally, allowing for multiple shots on different parts of the coated substrate.

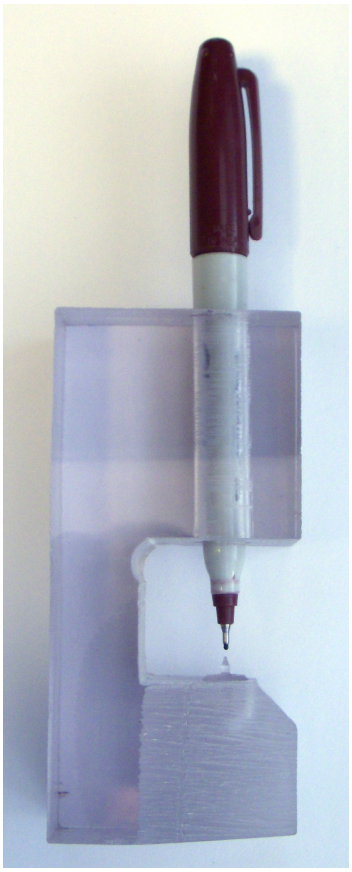

Figure 29: An apparatus created to ensure that the marker spot is directly opposite of the flyer location. The marker is aligned with the small point of plastic on the bottom so that when the flyer is centered on the plastic point, the marker will mark this position on the other side of the substrate.

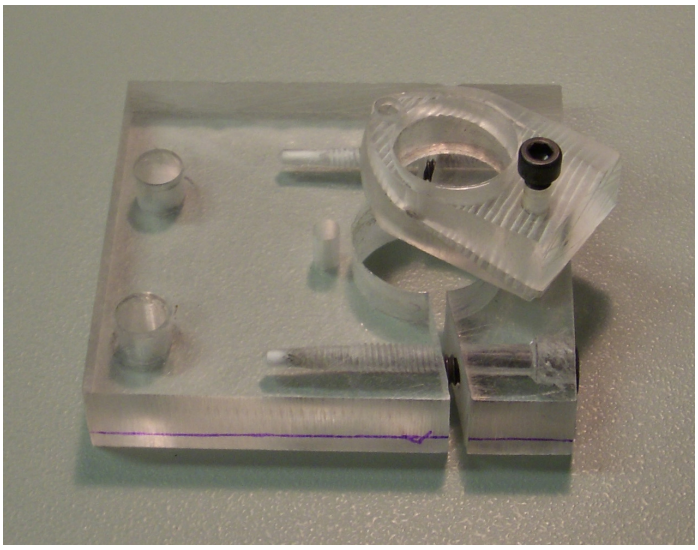

Figure 30: PMMA open air sample holder.

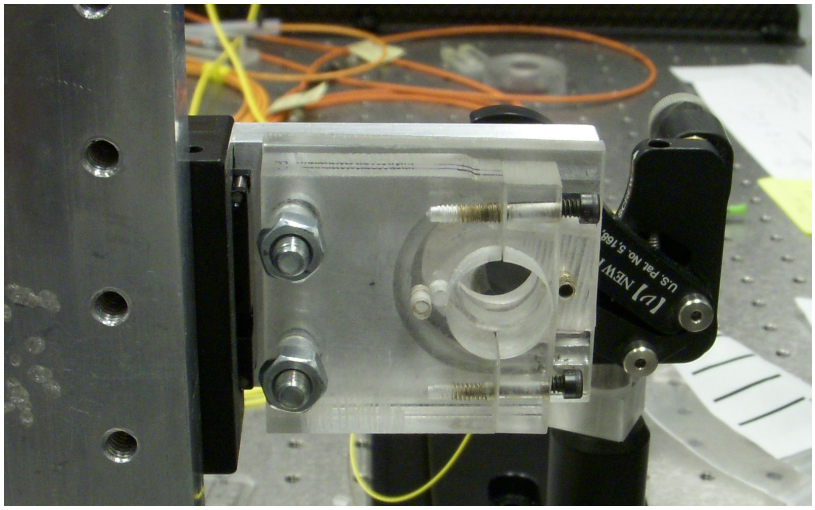

Figure 31: Single shot open air impact experiment chamber.

3.2.5 Flyer-Target Impact Experiment Chamber

A flyer-target impact experiment assembly was designed to hold the flyer and substrate assembly, as well as the target, if one is needed for the experiment, in a planar alignment. Lapped spacer rings are used to ensure that each component of the experiment assembly is held parallel to the others. Currently, the impact experiment assembly is designed for open air impacts as shown in Figure 30 and 31, but a container designed to be held under vacuum has been fabricated as well (shown in Figure 32). The vacuum-ready chamber is designed for single-shot experiments and is modeled after the chamber in use at Los Alamos National Laboratory. Figure 33 is the typical component layout inside of the vacuum chamber. The outer windows are sealed to the chamber itself with o-rings. All interior components are separated by lapped steel spacers. Both the open air and vacuum-ready chambers have a 19 mm diameter hole that holds the substrate/flyer assembly, spacer rings, and target.

The impact experiment assembly is placed in position before the beam converges to avoid dielectric breakdown in air. The last focusing lens has a focal length of 250 mm so the assembly must be less than 250 mm from the lens. To change the size of the irradiation spot, the lens can be moved closer to or farther from the impact

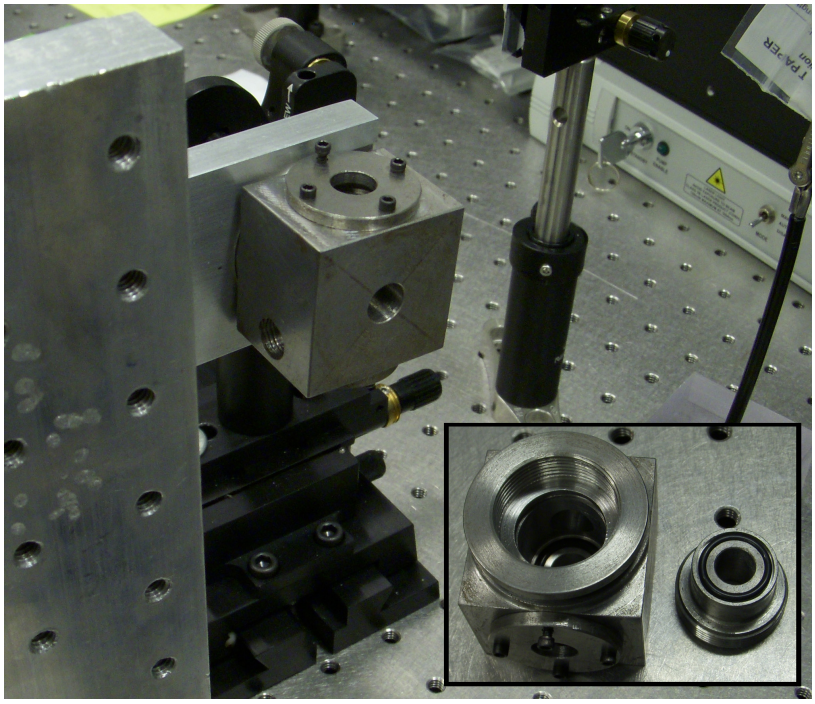

Figure 32: Impact experiment chamber designed to hold a vacuum.

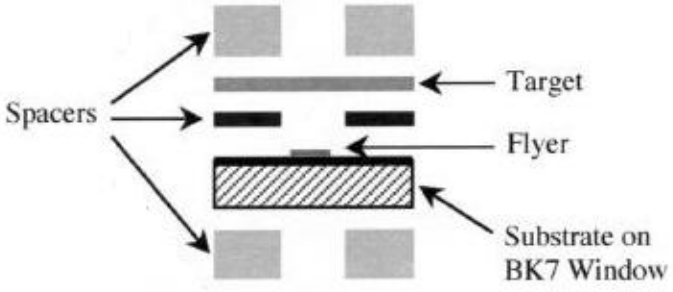

Figure 33: Typical set of components as assembled inside vacuum chamber (Robbins, 2004.

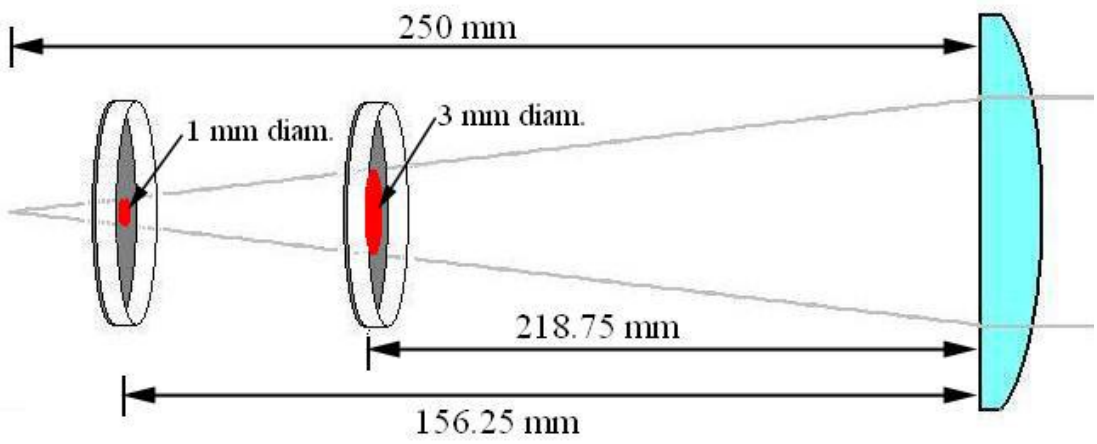

Figure 34: Beam spot size at different distances from the focal lens.

assembly. The beam exiting the beam shaper is 8 mm-diameter, so for a 3 mm spot size the distance between the lens and the interface between the substrate and the $C/Al_2O_3/Al$ coating should be 156.25 mm, or 5/8 of the total focal length away from the interface. For a 1 mm-diameter beam, the lens would be positioned 218.75 mm, or 7/8 of the total focal length away from the interface. Figure 34 graphically displays this concept.

3.3 PDV Setup

The PDV system consists of an IPG Photonics ELR-3-1550 SF 3 W single frequency Erbium Fiber Laser operating at a 1549.2 nm wavelength, the Bechtel Nevada Photonic Doppler Velocimeter (H-EO-61-B), and the Tektronix DPO 70804 Oscilloscope with 8 GHz bandwidth. The system bandwidth of the detector (12 GHz) and oscilloscope is 6.7 GHz. This means that the bandwidth limited maximum measurable velocity is 5200 $\frac{m}{s}$, well beyond the velocities created by the current laser system. The IPG laser beam is sent through an optical fiber to a 48 mm PDV focusing probe.

After ensuring that the PDV beam and alignment laser beam are aligned with each other, the substrate is mounted in front of the PDV probe. The IPG laser is turned on at its lowest power, and the amount of reflected light is maximized

by altering the tilt of the substrate, as well as the distance from the probe. After this optimization, the probe is backed away from the sample until the PDV system photodetectors reads -11 dBM. The power on the IPG laser is increased so that the PDV system reads around -4 dBM and then unshifted light is added until the PDV system has an average reading of -3 dBM. This process minimizes the harmonics that may be induced in the velocity profiles measured from PDV photodetector readings above 0 dBM.

The resulting beat frequency wave form is converted into DigSys files using MagPlot software. The DigSys files are analyzed using a Fast Fourier Transform in the pTool software. A window size of 5000 time points and a shift of 500 time points are used with a contrast minimum of -70 dB as a starting point for the transform. A total of 1000 points is equal to 400 ns. A smaller shift time yields better results, but is also more computationally intensive. Window size is a trade-off between certainty and velocity duration. Figure 35 shows PDV velocity traces revealing the effects of changing window size. At smaller window sizes (Figure 35a), many velocity components can be seen. As the window size is increased (Figure 35b), there is more certainty in the velocity because more cycles are counted in each window. As the window size is increased further (Figure 35c), the velocity curve starts to spread out, and if the window size is too large (Figure 35d), velocities with short duration are lost, and the velocity curve is too wide for accurate time data to be recorded. A velocity curve can be extracted from the profiles in Figure 35 by tracing around the velocity curve. pTool software then displays a velocity curve with the background noise removed, bandwidth, and uncertainty errors (Figure 36). Data can be saved in ASCII format for analysis in Excel.

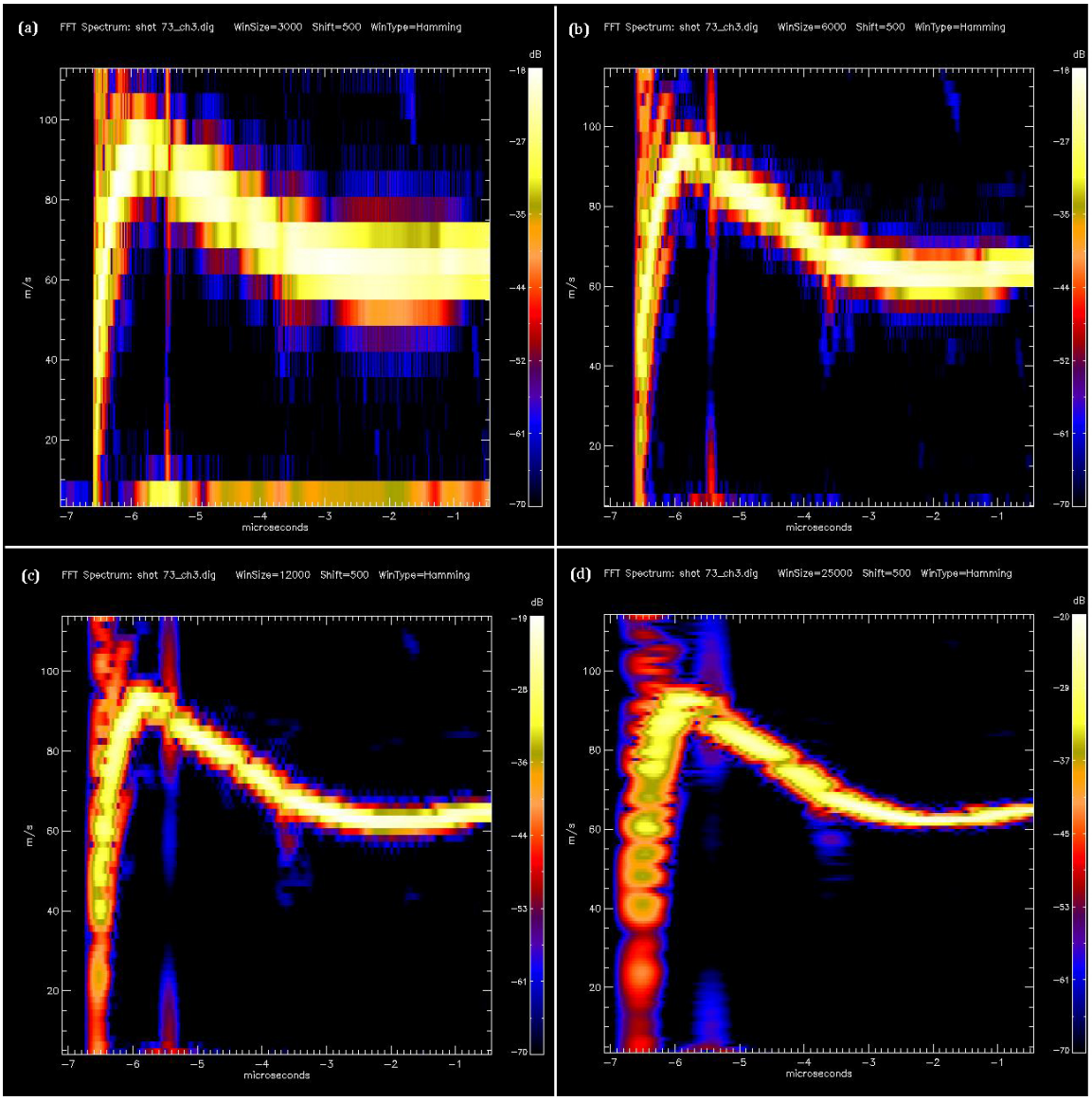

Figure 35: PDV velocity curves with varying window sizes: (a) window = 3000 time points, (b) window = 6000 time points, (c) window = 12000 time points, (d) window = 25000 time points.

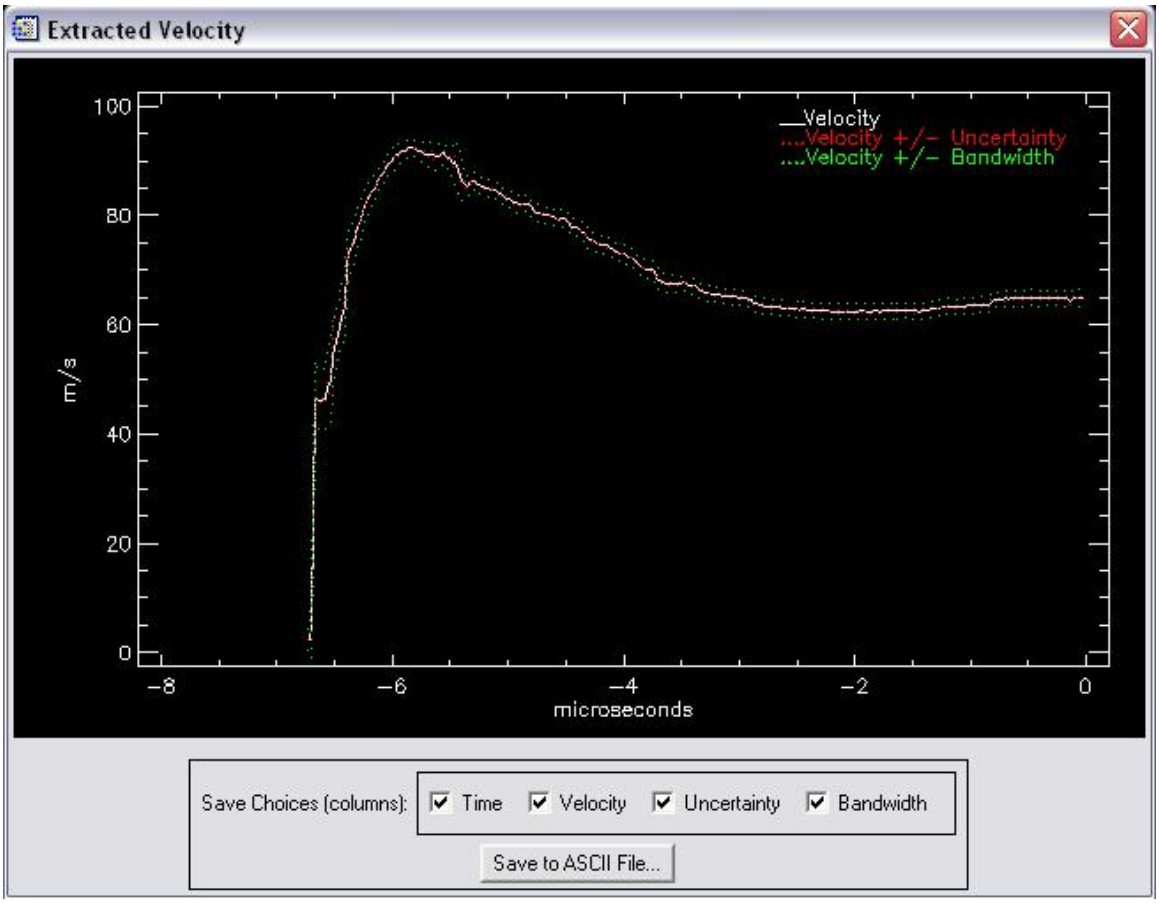

Figure 36: Velocity information is extracted by tracing the velocity curve. Data can be saved in ASCII format for analysis in Excel.

CHAPTER IV

REPRESENTATIVE MEASUREMENTS

The purpose of the research performed in this work was to set-up and characterize the performance of the laser-driven miniflyer system. Experiments were done using the laser system setup in which the 8 mm aperture was used for beam shaping. Flyers of 3.2 mm-diameter and 100, 50, or 25 μm thickness were used. Similar experiments were performed with flyers of 2.4 mm-diameter and 100, 50, or 25 μm thickness. To further characterize the laser-driven miniflyer system performance, experiments were also done using the laser system setup in which the refractive beam shaper was used. All work used PDV for velocity diagnostics, and the resulting velocity curves were used to determine conversion efficiency of the miniflyer system.

4.1 Flyer Velocity Profiles

Figures 37 and 38 show examples of typical velocity profiles for a 3.2 mm-diameter, 100 μm thick flyer irradiated with $\sim$ 900 mJ and a 2.4 mm-diameter, 25 μm-thick flyer irradiated with $\sim$ 900 mJ, respectively. The velocity profiles illustrate a rise to peak terminal velocity in $\sim 1\mu$s for both heavier (3.2 mm x 100 μm) and lighter (2.4 mm x 25 μm) copper flyers, accelerated with the same laser fluence. Initial rapid acceleration took place in $\sim$ 25 ns for both the heavier and lighter copper flyers. The temporal resolution of 10 ns of the PDV system is limiting in this analysis. The peak velocities obtained from these profiles were used to determine the effects of laser fluence and flyer mass, and, in turn, obtain the laser energy conversion efficiency. The velocity versus time profiles were also converted to velocity versus distance profiles to determine the distance over which the terminal velocity is attained.

In the experiments used to characterize the laser-driven miniflyer system, the

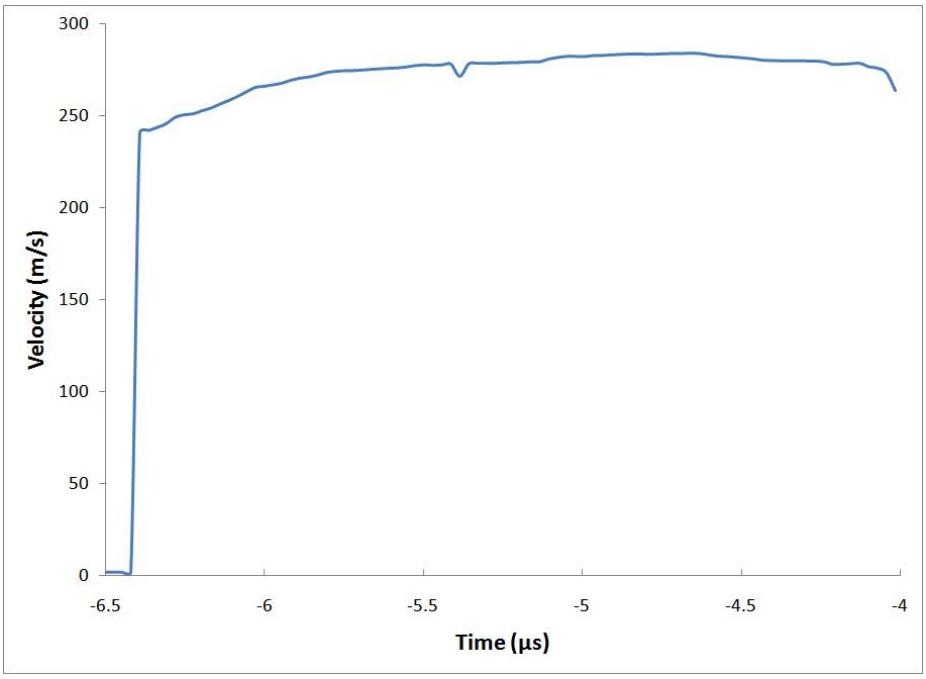

Figure 37: Flyer velocity versus laser pulse energy for 3.2 mm-diameter, 100 μm-thick flyer. Beam shaping done using an 8 mm aperture.

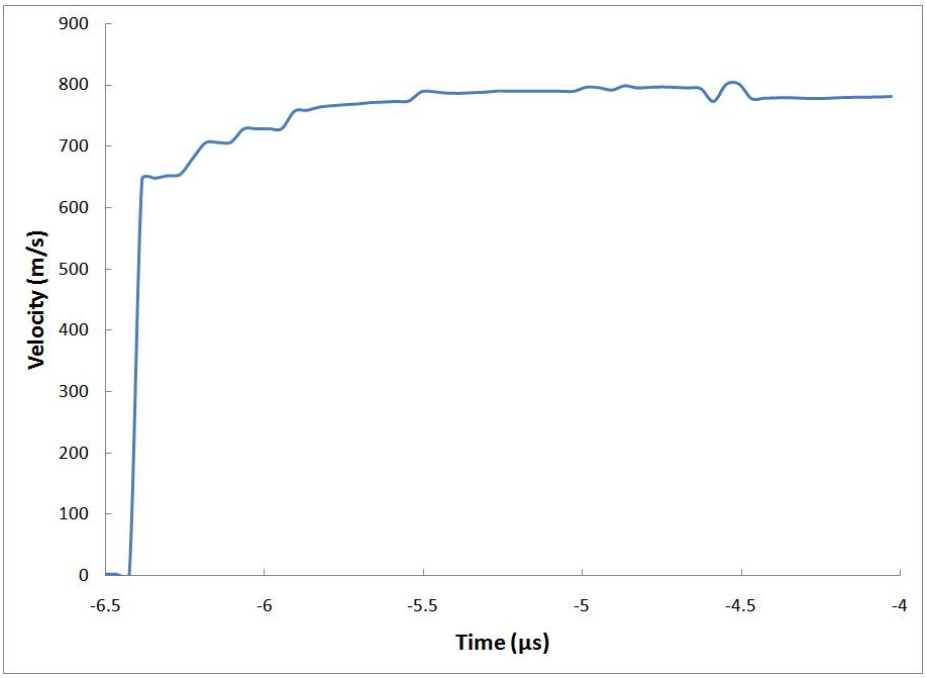

Figure 38: Flyer velocity versus laser pulse energy for 2.4 mm-diameter, 25 μm-thick flyer. Beam shaping done using an 8 mm aperture.

flyer was allowed to fly about 10 mm in order to get as complete a velocity profile as possible. This data is used to plot velocity and distance versus time, as well as velocity versus distance. With these plots, it can be determined at what time and distance the flyer reaches a steady state velocity. Figure 39 compares the distance traveled before steady-state velocity is reached for 100 μm-, 50 μm-, and 25 μm-thick flyers of both 3.2 mm- and 2.4 mm-diameter over a long distance. Figure 40 compares the distance traveled before steady-state velocity is reached for 100 μm-, 50 μm-, and 25 μm-thick flyers of both 3.2 mm- and 2.4 mm-diameter over the distance traveled during the initial launch of the flyers. This distance is dependent mainly on the final velocity that the flyer is able to achieve, which is based on the mass of the flyer (Table 2). As the mass decreases the flyer reaches a higher velocity and must travel farther before reaching that steady-state velocity. In this system, the acceleration of the flyers varies from $6.209x10^9$ $\frac{m}{s^2}$ for the heaviest flyers to $1.609x10^{10}$ $\frac{m}{s^2}$ for the lightest flyers. There are limits on the accuracy of this data as PDV is limited in tracking very high accelerations, but the behavior of the flyers is reasonable.

4.2 Effect of Driving Laser Energy

The characterization of the laser-driven miniflyer using velocity versus laser pulse energy provides essential information needed for further experiments in which flyer velocity information is needed but may not be directly measurable using PDV, such as in spall studies or impact experiments against non-transparent materials. In these cases, it is important that the accurate velocity of the flyer of given dimensions and mass for a particular laser pulse energy is available. Figures 41 and 42 are plots of the various velocity versus laser energy trends obtained in the characterization experiments for the laser system. It can be seen that the maximum velocities attained with maximum laser energy of 1.3J ranges from $\sim 250-700$ $\frac{m}{s}$ for the 3.2 mm-diameter flyers and $\sim 300-925$ $\frac{m}{s}$ for the 2.4 mm-diameter flyers.

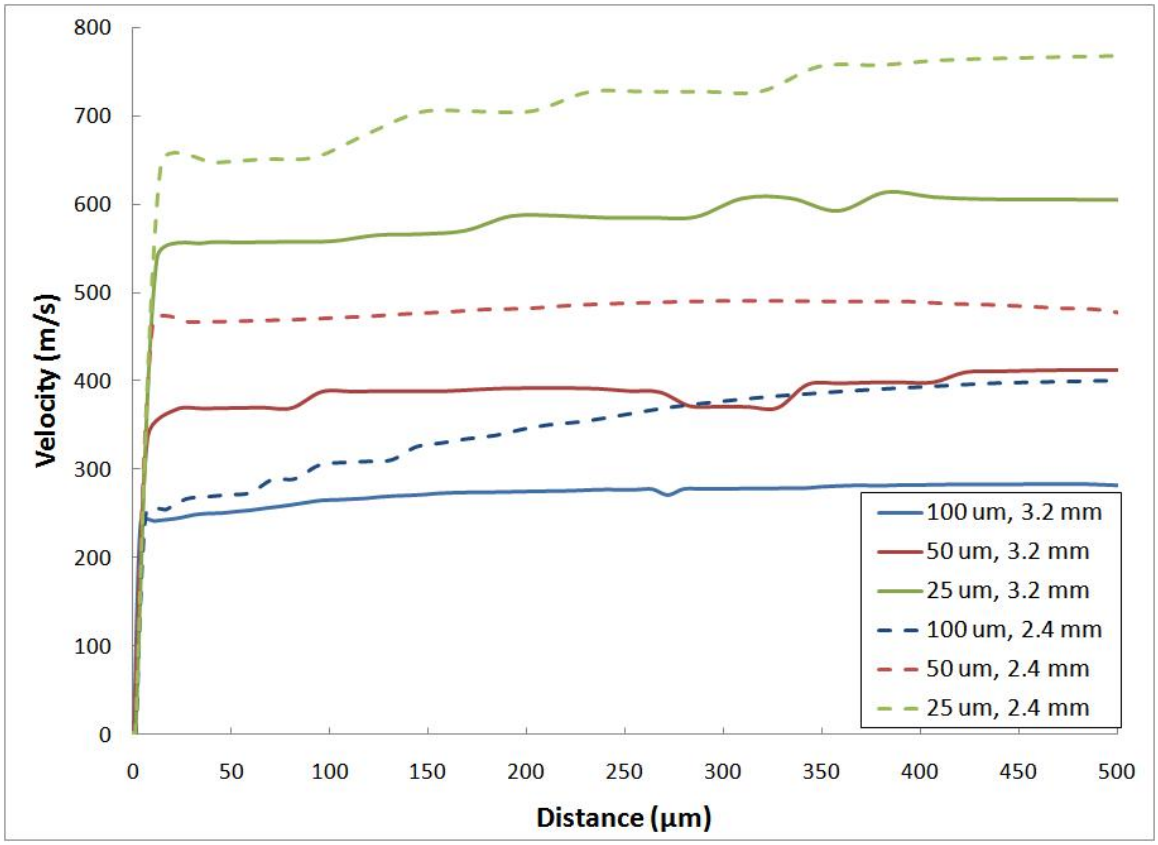

Figure 39: Velocity versus total distance traveled curves for ∼900 mJ shots on 3.2 mm- and 2.4 mm-diameter flyers of 100 μm, 50 μm, and 25 μm thickness. Beam shaping done using an 8 mm aperture.

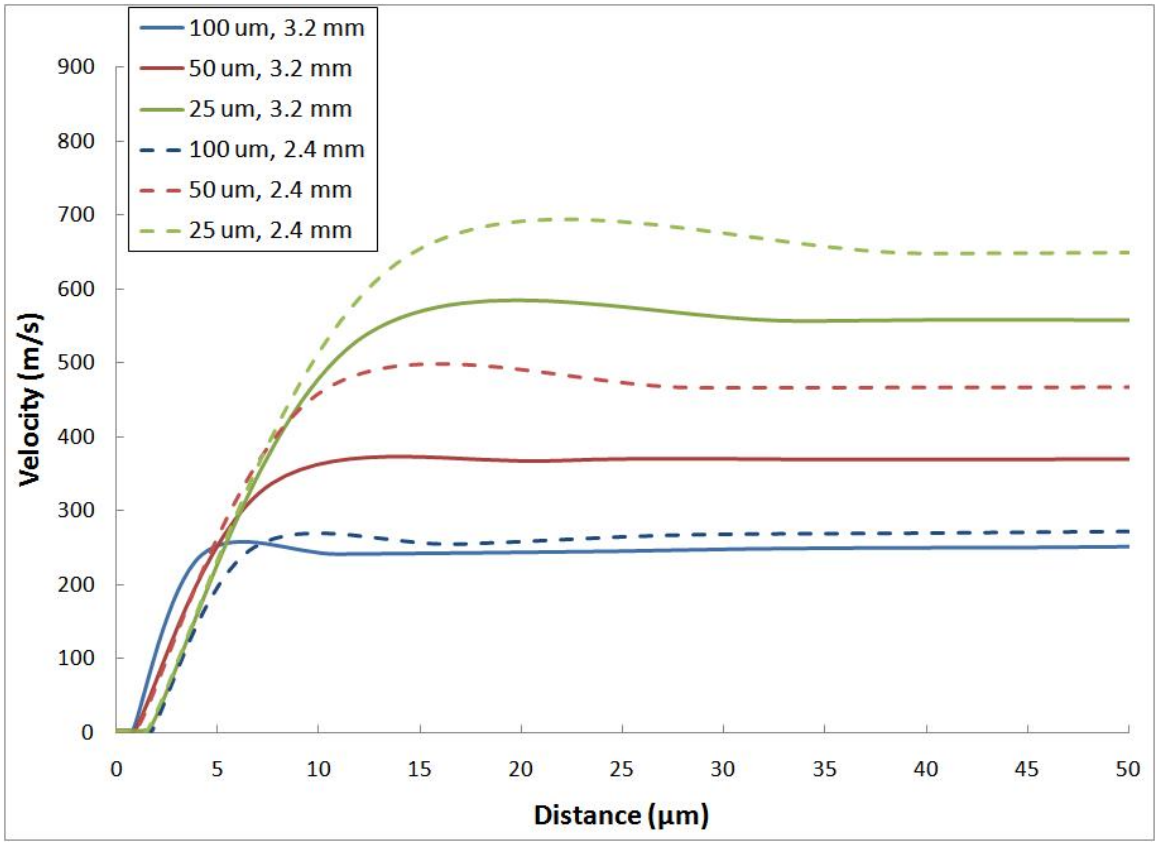

Figure 40: Velocity versus distance traveled during initial launch curves for ∼900 mJ shots on 3.2 mm- and 2.4 mm-diameter flyers of 100 μm, 50 μm, and 25 μm thickness. Beam shaping done using an 8 mm aperture.

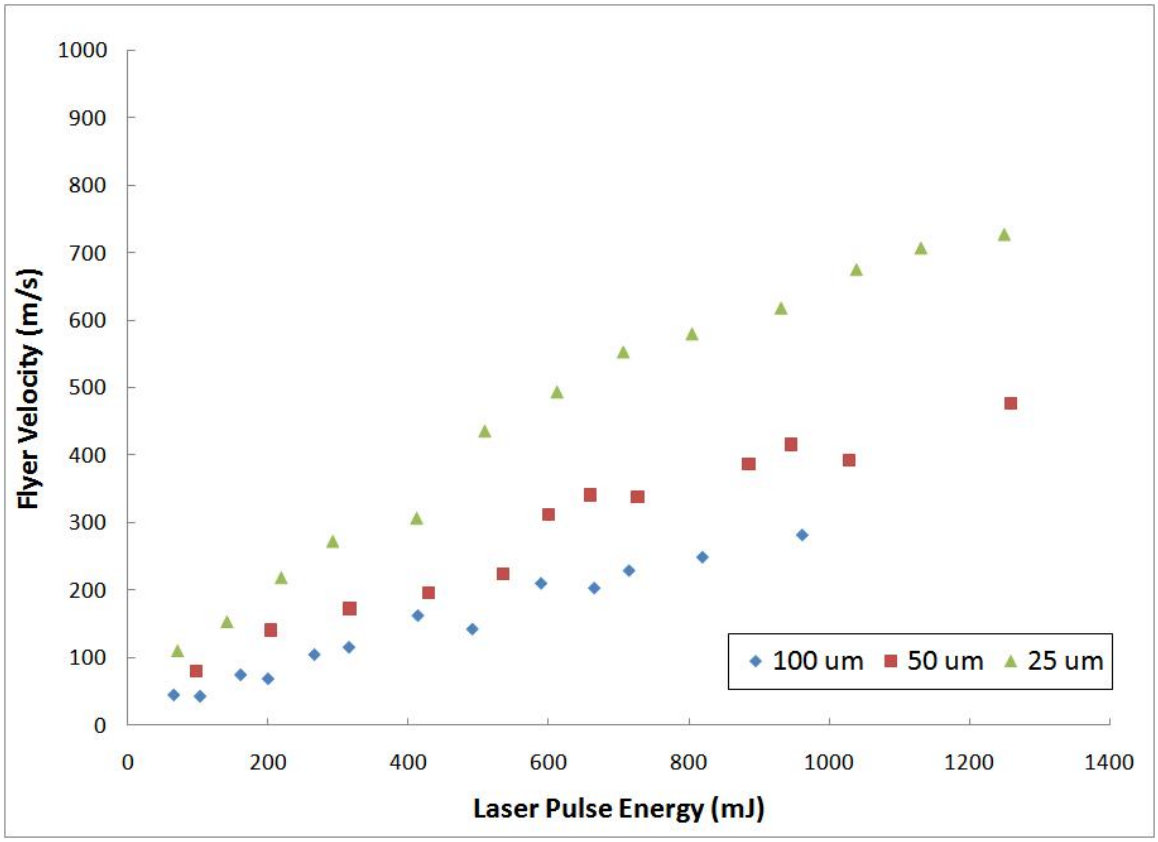

Figure 41: Flyer velocity versus laser pulse energy for 3.2 mm-diameter flyers in three thicknesses: 100 μm, 50 μm, and 25 μm. Beam shaping done using an 8 mm aperture.

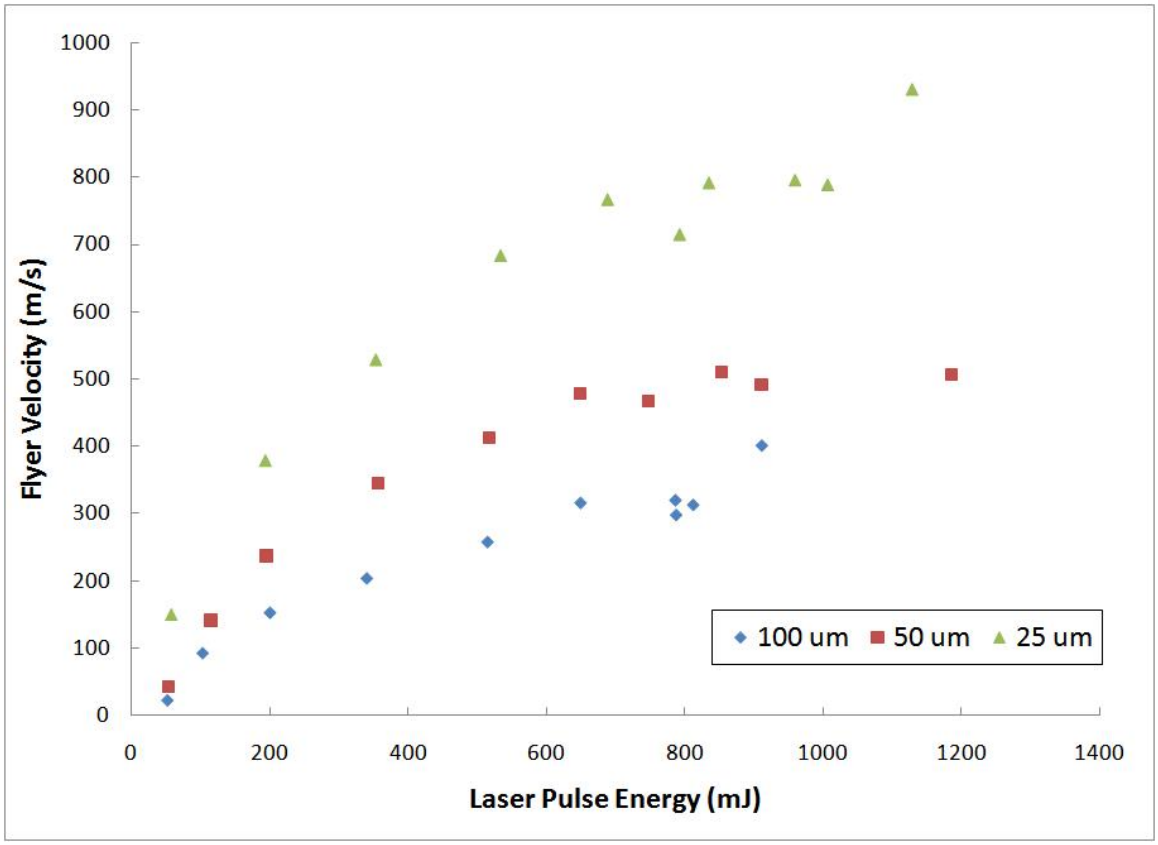

Figure 42: Flyer velocity versus laser pulse energy for 2.4-mm diameter flyers in three thicknesses: 100 μm, 50 μm, and 25 μm. Beam shaping done using an 8 mm aperture.

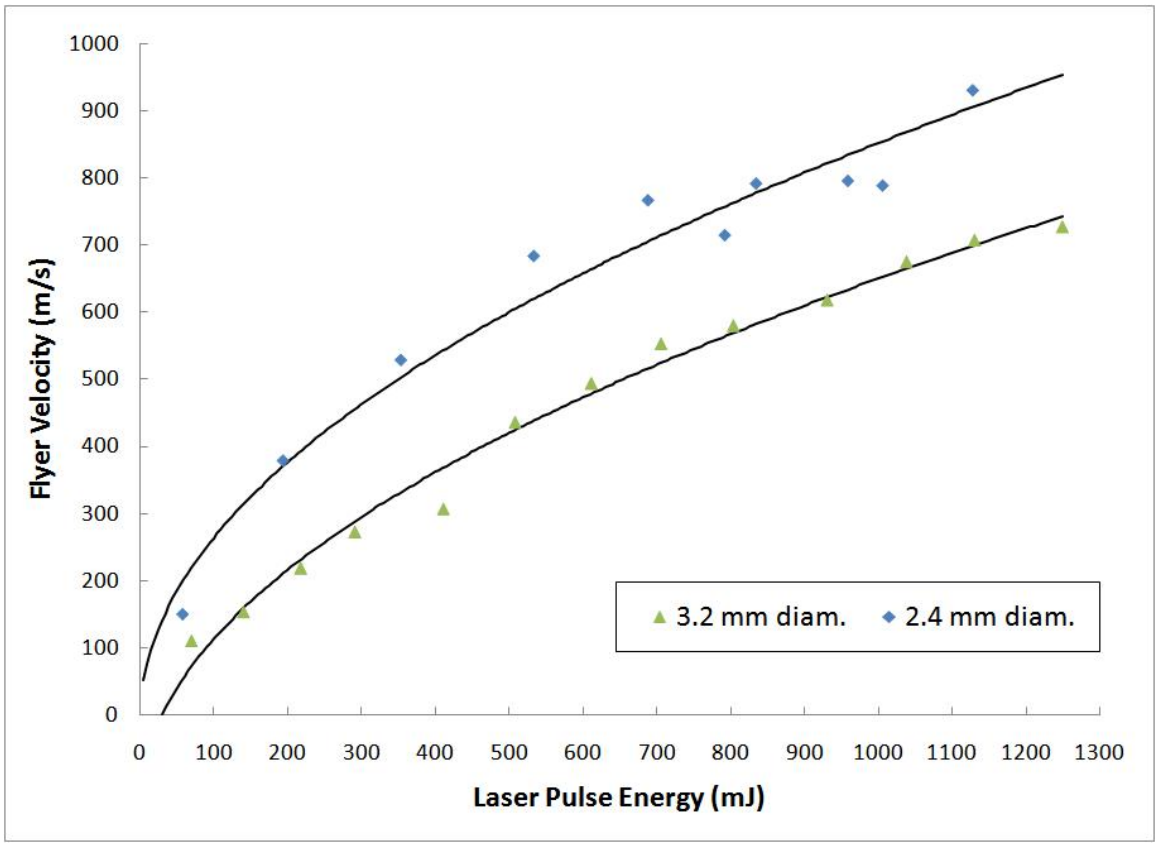

Figure 43: Flyer velocity versus laser pulse energy for 25 μm-thick flyers of 3.2- and 2.4 mm-diameter. Beam shaping done using an 8 mm aperture.

It is readily apparent that the change to a smaller diameter flyer affects the final velocity of the flyer. In following with conclusions drawn by Trott et al. [42], the flyer velocity varies with the square root of the mass of the flyer assuming constant conversion efficiency and laser pulse energy, $v = \sqrt{\frac{2kE}{m}}$. It can be seen in Figures 41 and 42 that as the mass doubles from 25 μm to 50 μm or 50 μm to 100 μm, the final velocity is roughly 70% lower. Looking at Figure 43 for 25 μm-thick flyers, it can be seen that the smaller diameter flyers are less consistent in their fit to a curve of the form $V = A\sqrt{E} - E_o$ with $A = \sqrt{\frac{2k}{m}}$. A similar trend can also be seen in the 50 μm- and 100 μm-thick flyers. The cause may be a higher concentration of laser power on the same substrate coatings causing ineffeciencies in launch or a misalignment of the smaller flyers with the PDV probe beam.

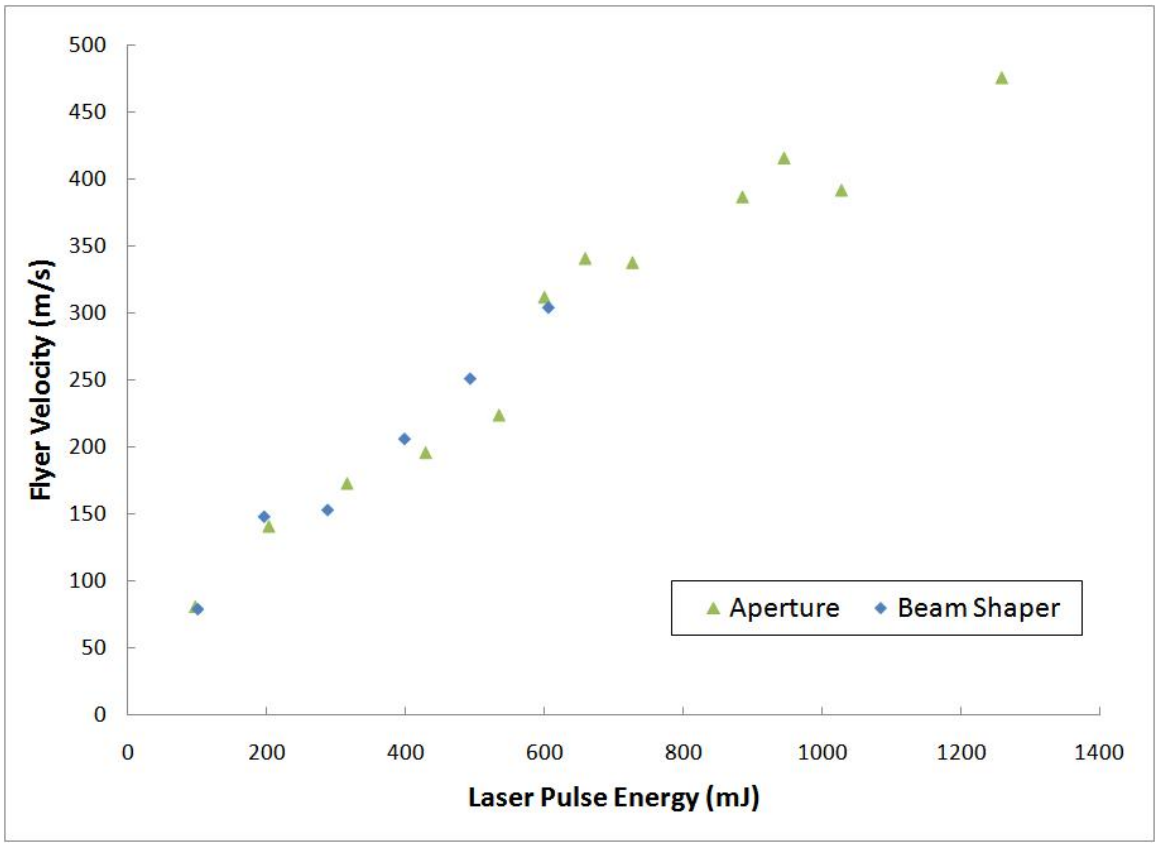

Figure 44: Plots of flyer velocity versus laser pulse energy for 50 μm-thick, 3.2 mm-diameter flyers comparing beam shaping done with a refractive beam shaper and beam shaping done using an 8 mm aperture.

While the velocity trends revealed in Figures 37 - 43 employed the 8 mm aperture for beam shaping, experiments were also done to investigate the effects of replacing the 8 mm aperture with the refractive beam shaper. However, because of the damage threshold of the beam shaper, input laser energy was limited to under 700 mJ. The comparison of data in Figure 44 shows that the beam shaper has no substantial impact on the final velocity of the miniflyer for the case of the 50 μm-thick, 3.2 mm-diameter flyers. Further experiments with imaging techniques are needed to obtain knowledge of the planarity of the flyer with and without the beam shaper. It may be advantageous to use the 8 mm aperture because of the unlimited damage threshold.

Table 2: Average flyer mass, minimum launch energy and conversion efficiency for each flyer setup.

Flyer Diameter	Flyer Thickness	Average Flyer Mass	Minimum Launch Energy	Conversion Efficiency
3.2 mm	100 μm	0.00726 g	38 mJ	43%
3.2 mm	50 μm	0.00441 g	38 mJ	46%
3.2 mm	25 μm	0.00359 g	30 mJ	55%
2.4 mm	100 μm	0.00221 g	18 mJ	42%
2.4 mm	50 μm	0.00177 g	4 mJ	36%
2.4 mm	25 μm	0.00097 g	0.15 mJ	36%

4.2.1 Conversion Efficiency

An important performance attribute of the laser-driven miniflyer system is the conversion efficiency of the Nd:YAG laser into kinetic energy of the flyer. There are many parameters that can affect this efficiency; two of which are window material and substrate coating. The laser-driven miniflyer setup used in the High Strain Rate Lab and based on the setup at Los Alamos National Laboratory [27] employed commercial-grade BK7 as the window material and a composite coating of 0.5 μm carbon, 0.5 μm aluminum oxide, and 1.5 μm aluminum on the substrate.

As with studies by Sheffield et al. [31], Trott et al. [42], and Robbins et al. [27], the relationship between velocity and energy is expected from a model where total energy is conserved and the foil kinetic energy is equated to the laser energy multiplied by a conversion efficiency constant. To calculate this conversion efficiency, k, the measured peak velocity is plotted as a function of the square root of the laser pulse energy (Figure 45). A linear regression line fit to the data points yields the slope, m, equivalent to $\sqrt{\frac{2k}{m}}$. Once k is determined a least-squares fit of the form $V = A\sqrt{E} - E_o$ with $A = \sqrt{\frac{2k}{m}}$ can then be fit to the original data trends of velocity versus laser pulse energy.

Figures 46 and 47 plot the velocity versus laser pulse energy for 3.2 mm- and 2.4

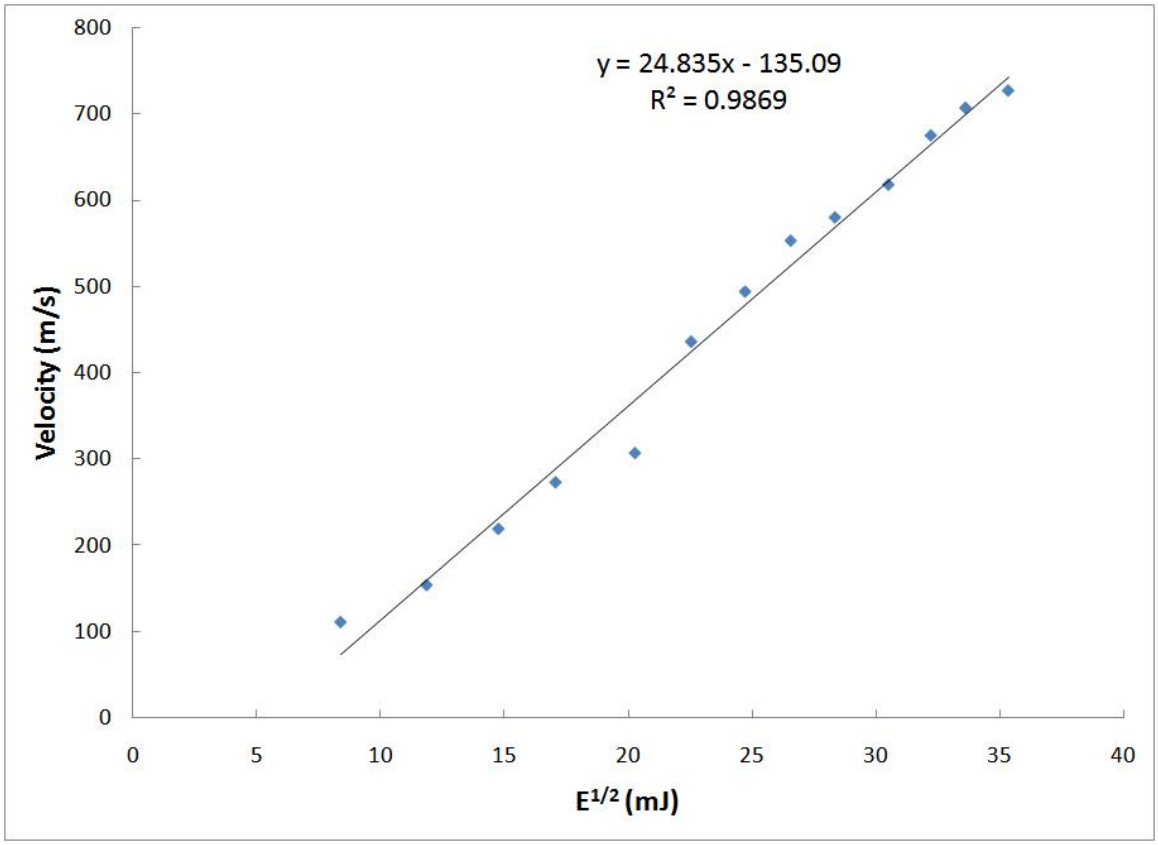

Figure 45: Plot of velocity versus the square root of laser pulse energy for 3.2 mm-diameter, 25 μm-thick flyers. A linear regression is used to find the conversion efficiency, k, for the system.

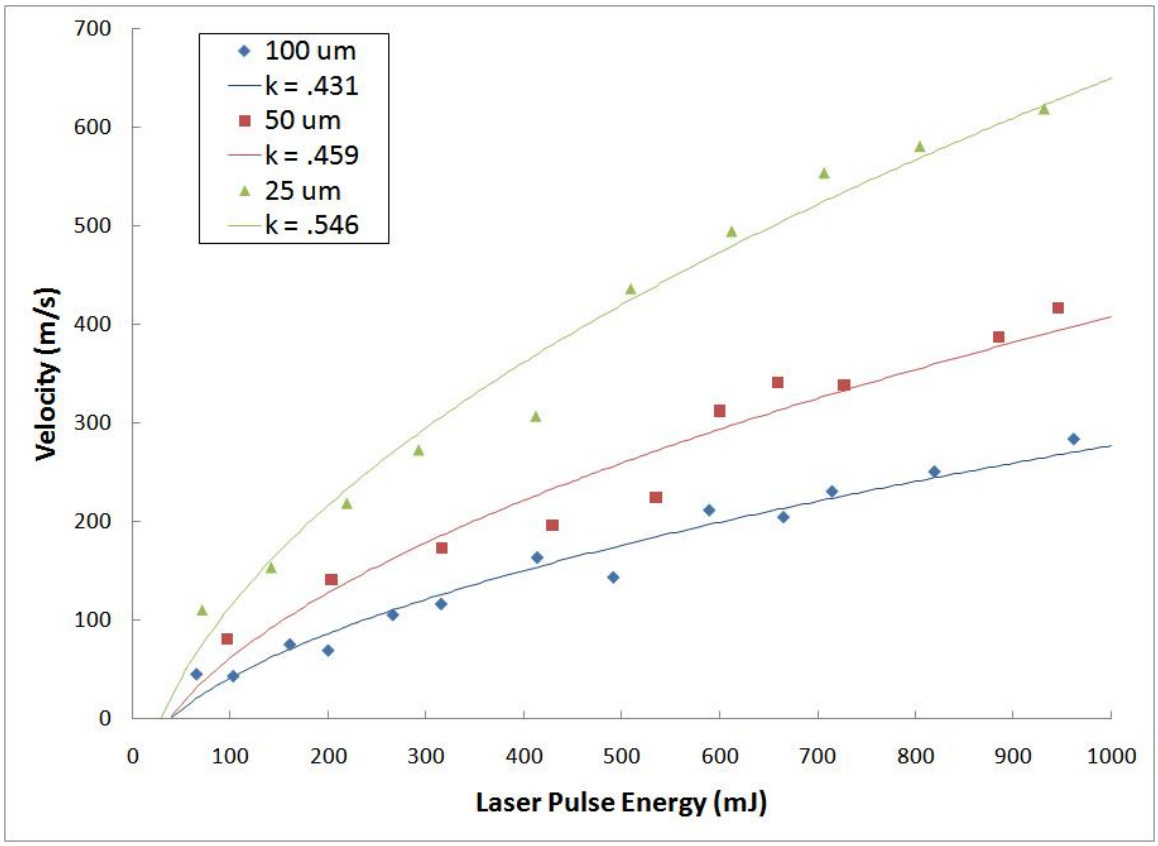

Figure 46: Plots of flyer velocity versus laser pulse energy with k curve fit for 3.2 mm-diameter flyers in three thicknesses: 100 μm, 50 μm, and 25 μm. Beam shaping done using an 8 mm aperture.

mm-diameter flyers of 100 μm, 50 μm, and 25 μm thickness. As can be seen from the plots, the minimum energy required to launch a particular flyer can be determined from the $V = 0$ intercept of the curve. This value corresponds to E_o in the model equation. The values of the minimum energy to launch a flyer are shown in Table 2. The order of these values of conversion efficiencies is expected as it takes more energy to launch a flyer with more mass.

The conversion efficiency of the laser-driven miniflyer setup in the High Strain Rate Lab at Georgia Tech with the Continuum Powerlite II Plus laser surpasses many recorded values by other research teams. Sheffield et al. [31] reached a conversion efficiency of 25% for 66 μm-thick aluminum flyers of 1.5 mm-diameter. Trott et al. [42] found k values approaching 35% for both 12.7 μm- and 5 μm-thick aluminum

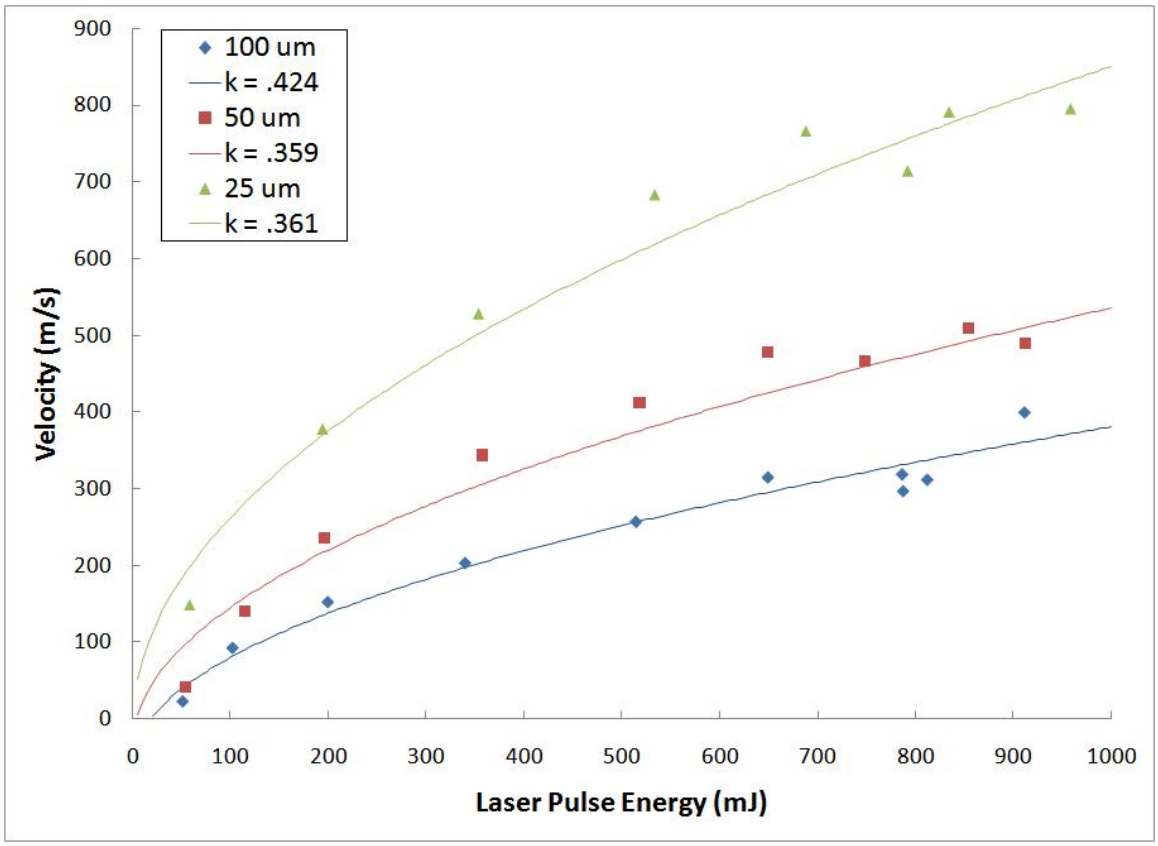

Figure 47: Plots of flyer velocity versus laser pulse energy with k curve fit for 2.4 mm-diameter flyers in three thicknesses: 100 μm, 50 μm, and 25 μm. Beam shaping done using an 8 mm aperture.

foils directly coupled to the output face of 0.2 mm to 1.0 mm diameter fiber optic cables. Robbins et al. [27] calculated a conversion efficiency of 14% for 3 mm-diameter, 50 μm-thick copper flyers. The lowest conversion efficiency value from current characterization experiments in the High Strain Rate Laboratory was 36%, and the highest conversion efficiency was 55%. Figure 48 displays the efficiency results from our current experiments, as well as the data point from Robbins et al. [27].

The 3.2 mm-diameter flyers have a higher conversion efficiency, except for the 100 μm-thick flyer. Shots done above 700 mJ of laser pulse energy with the 100 μm-thick flyers resulted in small discs of BK7 roughly equal to the size of the flyer but half the mass broke free from the substrate on the side of the incoming laser pulse. These discs had considerable velocity in the opposite direction of the flyer velocity, which may

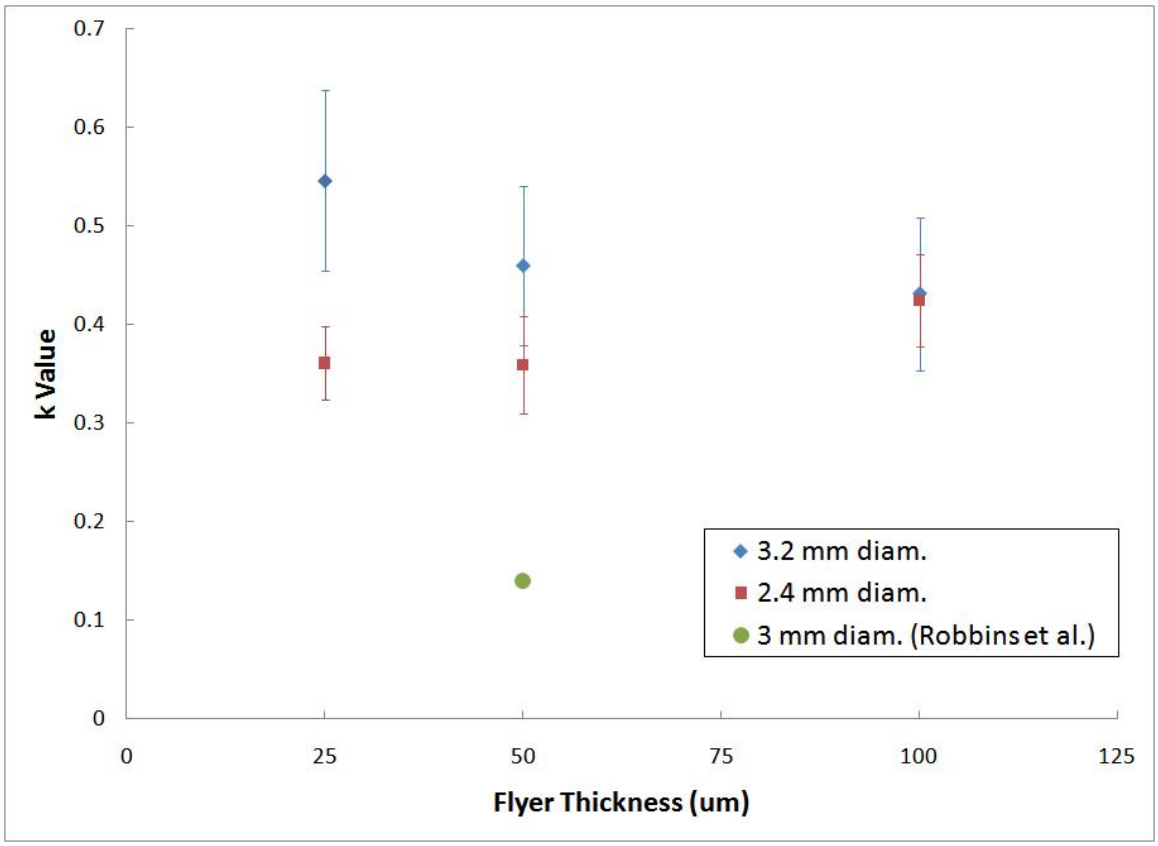

Figure 48: Conversion efficiency, k, for each flyer setup versus flyer thickness. Error is based on the farthest point from the linear fit to the plot of velocity versus square root of laser pulse energy.

explain the lower conversion efficiency as some of the laser pulse energy can be lost in the breaking of the BK7 substrate and the kinetic energy of the flying BK7 disc. This phenomenon was only seen with the 100 μm-thick, 3.2 mm-diameter flyers due to the increased mass. To increase the efficiency of these shots thicker BK7 substrates can be used that better resist breaking under the pressure of the expanding plasma.

The higher values of conversion efficiency are most likely due to variations in substrate coating techniques and finishes, flyer creation techniques, or flyer attachment techniques from other laboratories' setups. Of these, it is difficult to determine the exact reason for the increases in conversion efficiency without direct comparison with other laboratories' setup techniques.

CHAPTER V

SUMMARY OF RESULTS AND RECOMMENDATIONS

5.1 Results

The research performed in the set-up and characterization of the laser-driven miniflyer system included the (i) investigation of two different beam shaping methods; (ii) optimization of the PDV diagnostic system for flyer velocity measurements; (iii) characterization of the laser system using effect of laser energy and flyer mass on velocity profiles; and (iv) identification of the system conversion efficiencies.

(i) Investigation was done to determine which beam shaping method best created a top hat profile while also allowing for the maximum possible laser beam pulse energy to impact the substrate. It was determined that both the refractive beam shaper and the 8 mm aperture created similar top hat profiles. The velocity versus laser pulse energy plots for each beam shaping method were nearly identical, but the beam shaper was limited to an output of 900 mJ while 1250 mJ were able to be sent through the aperture.

(ii) The PDV system is a relatively simple tool for the laser-driven miniflyer system diagnostics. Issues can arise from harmonic velocity curves above the desired curve, as well as varying reflections that can result in lost or weakened beat frequency wave form. A reflection intensity of -11 dBM with minimum laser power and no unshifted light was shown to be an optimal starting point. Roughly 0.3 W of laser power was able to be added to bring the photodetector reading to -4 dBM, allowing for strong enough reflection off of the flyer in cases of misalignment during flight. A small amount of unshifted light was then added to bring the the average photodetector reading to -3 dBM. Regarding the Fast

Fourier Transform in the pTool software, a window size to time shift ratio of 10:1 was found to be a good starting point for generating an accurate, easy-to-read velocity curve.

(iii) Characterization of the laser system using the velocity profiles generated from over 100 shots provided valuable information regarding the behavior of flyers of varying thickness and diameter. Flyer velocity was found to be related to the square root of the mass of the flyer. Copper flyers of 2.4 mm-diameter and 25 μm-thickness were found to reach the highest velocities for a given laser energy, but overall, the 2.4 mm-diameter flyers exhibited less predictable velocities than the 3.2 mm-diameter flyers. This was seen in the lower average R^2 value for curve fits to the 2.4 mm diameter velocity versus laser energy trends.

(iv) Overall, conversion efficiencies were higher than previously reported values, but it is difficult to determine the exact reason for the increases in conversion efficiency for other laboratories' setups without direct comparison to their techniques. The higher values of conversion efficiency are most likely due to variations in substrate coating techniques and finishes, flyer creation techniques, or flyer attachment techniques. Copper flyers of 3.2 mm-diameter averaged higher conversion efficiencies than the 2.4 mm-diameter flyers, perhaps due to a larger laser irradiation spot. Smaller irradiation area may have lead to more fracture of the BK7 substrate, resulting in lower conversion efficiency from laser energy to kinetic energy of the flyer.

5.2 Recommendations

Recommendations regarding (i) beam shaping methods; (ii) optimization of the velocity diagnostic system; and (iii) flyer design are as follows:

(i) The refractive beam shaper, when aligned perfectly, generates a marginally

better flat top profile than with the use of an aperture, but it is limited by a 10 $\frac{J}{cm^2}$ damage threshold. For higher power experiments, the beam shaper must be removed from the system and replaced with the aperture. Future additions to the laser-driven miniflyer system could be a diffuse diffractive optical beam shaper such as the one used by Los Alamos National Laboratories (MEMS Optical Inc.). The damage threshold for these devices is limited by the fused silica from which they are made. Damage thresholds of $3850\frac{J}{cm^2}$ for 8 ns pulses from a single-mode Q-switched laser have been found for the fused silica [32]. The element is also optically loss-less because it is purely a phase mask. Further experiments with imaging techniques are needed to obtain knowledge of the planarity of the flyer with and without the beam shaper.

(ii) The PDV system settings can be tailored to a variety of experimental setups. For the laser-driven miniflyer system, setting the IPG laser at a power above 0.3 W helps to ensure that enough light is reflected back into the PDV probe even if the flight of the flyer is irregular or tilted. This can be done by finding the maximum reflection into the probe at minimum PDV laser power and then backing out the probe until the photodetectors read less than -11 dBM. Better PDV readings were also found with setups that had less added-in unshifted light rather than more. The unshifted light should only raise the total amount of collected light at the photodetector about 1-2 dBM.

For analysis of initial acceleration profiles, VISAR is desirable because of its temporal resolution of 1 ns compared to the temporal resolution of 10 ns for PDV. In this way, small fluctuations in acceleration during the initial rapid acceleration will be seen.

(iii) Flyer design regarding thickness and diameter is subjective, but given the results of conversion efficiency, 3.2 mm-diameter flyers are somewhat more efficient in

launch. During flight, the size of the 3.2-mm diameter flyers make it easier to get a PDV trace. These flyers may have more area to generate air resistance, but in the long term, the use of an evacuated experiment chamber can eliminate this issue. Given that the 3.2 mm-diameter copper flyers are easier to handle, and have a better fit to the velocity versus energy trends, they are recommended for use with future impact experiments.

APPENDIX A

OPERATION MANUAL FOR LASER-DRIVEN MINIFLYER SYSTEM

A.1 Start-up

(i) Open city water and drain source connected to laser system (red handle should be in line with pipe when open)

(ii) Ensure the 24V power supply switch located on rear of electronics cabinet is **ON**.

(iii) Switch on electronics rack circuit breaker located on the right hand side of the front of the cabinet. The CG604C pump will also turn on.

(iv) Turn key on front panel of CU601C counter-clockwise to the **ON** position.

(v) Flip the power switch on the back of the seed laser to the **ON** position and the key to the **ON** position. Flip the mode switch to **DSBL**.

(vi) After approximately 15 seconds the control unit will complete its system check and countdown. The phrase **MANUAL MODE** is then displayed on the remote box RB601.

(vii) Log the shot count in the laser logbook.

(viii) Press the **AUTO/MANUAL** key on the remote box and ensure that PGM1 (FLASH ONLY) is displayed on the screen. Then press the **START** key.

(ix) The laser heads will now be flashing at the standard repetition rate of 10 Hz.

(x) Allow the system to run for 30 minutes without Q-switching to thermally stabilize the system (check the water temperature to ensure proper operating temperature at 87-90°F).

A.2 Firing

(i) Put laser protective eyewear on.

(ii) Turn the laser safety sign on (light on switch should turn on).

(iii) Open the port on the front of the Nd:YAG laser.

(iv) Open the 1064 nm wavelength port by pulling the knob on the top of the laser closest to the door.

(v) Select the desired programmed mode of operation by pressing the **PROGRAM UP** key on the control box.

(vi) Once the desired PGM is located press the **ACTIVATE** key to engage the PGM.

(vii) Flip the mode switch on the seeder laser from **DSBL** to **AUTO**.

(viii) On the control box press the **shutter** key to open the shutter and the **Q-SWITCH** key to activate Q-switching (begin lasing). The four LEDs across the top of the control box should be flashing.

A.3 Alignment

(i) Set up two adjustable apertures (available at Edmund Optics - High Performance Standard Series Iris Diaphragms) with a gap between them directly in front of the Powerlite beam. A bigger gap between the apertures ensures better alignment.

(ii) Turn the laser on so it is firing at its standard rep rate. Ensure that it is emitting at low power.

(iii) Using an IR card, align the first aperture (at its most open setting) to the beam by moving the aperture until the beam comes completely through.

(iv) Close the first aperture somewhat and align the second aperture so that the beam is centered in the aperture.

(v) Continue this process until the beam passes through both apertures at their smallest setting.

(vi) Lock the apertures in place.

(vii) Using the alignment laser beam steerer (available from Newport) and a mirror that reflects the alignment beam while allowing the Powerlite beam to pass (Newport High-Energy Nd:YAG Harmonic Beamsplitter) to align the alignment laser so that it passes through both apertures at their smallest setting (do not move the apertures).

(viii) When the alignment beam and the Powerlite beam both pass through the apertures they are in alignment.

(ix) Add one optic to the beam path at a time. Check alignment after each optic.

(x) After each optic, mount a piece of burn paper and shoot with the Powerlite. Check to ensure that the alignment laser beam is centered on the burn spot. If it isn't, adjust the alignment laser positioning using the 2 mirror alignment beam steerer.

(xi) Mount burn paper to a ruler or stand and do a shot at each point of system to determine height changes as well. The beam should remain close to parallel with the laser table.

(xii) Check the alignment and beam size of the area to be irradiated by mounting a piece of burn paper in the experiment chamber. Ensure that the alignment laser marks the center of the burn pattern and that the radius of the beam pattern is the correct size for the flyer being launched.

A.4 Shut-down

(i) Press the **STOP** key on the control box.

(ii) Close the port on the front of the Nd:YAG laser.

(iii) Close the 1064 nm wavelength port on the top of the laser.

(iv) Leave the seeder power on. Turn the key from **ON** to **STBY**. Flip mode switch to **DSBL**.

(v) Turn key on front panel of the cabinet clockwise to the **OFF** position.

(vi) Flip the power switch on the back of the seeder laser to **OFF** position.

(vii) Leave the 24 V power supply switch on rear of electronics rack in the **ON** position.

(viii) Switch off the electronics rack circuit breaker located on front right hand side of cabinet (power lights may take $\sim$20 seconds to go out).

(ix) Close city water and drain source connected to the laser system (red handle should be perpendicular to the water pipe).

REFERENCES

[1] Asay, J. R., "Sandia National Laboratories Report SAND81-1901," tech. rep., The Sandia National Laboratories Shock Thermodynamics Applied Research Facility, 1981.

[2] Asay, J. R. and Shahinpoort, M., eds., *High-Pressure Shock Compression of Solids*. Springer-Verlag, 1 ed., 1993.

[3] Barker, L. M. and Hollenbach, R. E., "Laser Interferometer for Measuring High Velocities of any Reflecting Surface," *Journal of Applied Physics*, vol. 43, no. 11, pp. 4669–4675, 1972.

[4] Barnes, N. P. and Barnes, J. C., "Injection Seeding I: Theory," *IEEE Journal of Quantum Electronics*, vol. 29, pp. 2670–2683, 1993.

[5] Cogan, S., Shirman, E., and Haas, Y., "Production efficiency of thin metal flyers formed by laser ablation," *Journal of Applied Physics*, vol. 97, no. 11, p. 113508, 2005.

[6] Continuum, "Continuum Powerlite Precision II 9000 Data Sheet," 2004.

[7] Dickey, F. M., Weichman, L. S., and Shagam, R. N., "Laser beam shaping techniques," *High-Power Laser Ablation III*, vol. 4065, no. 1, pp. 338–348, 2000.

[8] Goodman, J. W., *Introduction to Fourier Optics*. Roberts and Company Publishers, 2004.

[9] Gurney, R. W., "The Initial Velocities of Fragments from Bombs, Shell, Grenades," Tech. Rep. 405, Ballistic Research Laboratories, Aberdeen Proving Ground, MD, 1943.

[10] Hatt, D. J. and Waschl, J. A., "A study of laser-driven flyer plates," in *Shock Compression of Condensed Matter*, vol. 370, pp. 1221–1224, American Physical Society Topical Conference Proceedings, May 1996.

[11] He, H., Kobayashi, T., and Sekine, T., "Time-resolved measurement on ablative acceleration of foil plates driven by pulsed laser beam," *Review of Scientific Instruments*, vol. 72, no. 4, pp. 2032–2035, 2001.

[12] Hemsing, W. F., "Velocity sensing interferometer (visar) modification," *Review of Scientific Instruments*, vol. 50, no. 1, pp. 73–78, 1979.

[13] Hoffnagle, J. A. and Jefferson, C. M., "Beam shaping with a plano-aspheric lens pair," *Optical Engineering*, vol. 42, no. 11, pp. 3090–3099, 2003.

[14] Hongo, T., Matsuda, A., Kondo, K., Nakamura, K., and Atou, T., "Flyer Acceleration by Pulsed Laser and its Application to Shock-Recovery Experiment on MnF_2," *Japanese Journal of Applied Physics*, vol. 44, no. 7A, pp. 5006–5008, 2005.

[15] Ito, K. and Aizawa, T., "Laser Shock Loading Device for Real Time Evaluation of Shock Induced Reaction," *Journal of Materials Processing Technology*, vol. 85, pp. 91–96, 1999.

[16] Kalantar, D. H., Chandler, E. A., Colvin, J. D., Lee, R., Remington, B. A., Weber, S. V., Wiley, L. G., Hauer, A., Wark, J. S., Loveridge, A., Failor, B. H., Meyers, M. A., and Ravichandran, G., "Transient x-ray diffraction used to diagnose shock compressed si crystals on the nova laser," in *Review of Scientific Instruments*, vol. 70, pp. 629–632, AIP, 1999.

[17] Kaufman, M. I., Malone, R. M., Frogget, B. C., Esquibel, D. L., Romero, V. T., Lare, G. A., Briggs, B., Iverson, A. J., Frayer, D. K., DeVore, D., Cata, B., Holtkamp, D. B., Wilke, M. D., King, N. S. P., Furlanetto, M. R., Briggs, M. E., and Furnish, M. D., "Design, construction, alignment, and calibration of a compact velocimetry experiment," in *Optical System Alignment and Tolerancing* (Sasian, J. M. and Ruda, M. C., eds.), vol. 6676, p. 667607, SPIE, 2007.

[18] Kennedy, J. E., "Gurney Energy of Explosives: Estimation of the Velocity and Impulse Imparted to Driven Metal," Tech. Rep. SC-RR-70-790, Sandia Laboratories, Albuquerque, NM, 1970.

[19] Lawrence, R. J., "The equivalence of simple models for radiation-induced impulse," in *Shock Compression of Condensed Matter*, American Physical Society Topical Conference Proceedings, January 1991.

[20] Lawrence, R. J. and Trott, W. M., "Theoretical Analysis of a Pulsed-Laser-Driven Hypervelocity Flyer Launcher," *International Journal of Impact Engineering*, vol. 14, pp. 439–449, 1993.

[21] Moore, D. S., McGrane, S. D., and Funk, D. J., "Ultrashort laser shock dynamics," in *ShockWave Science and Technology* (Horie, Y., ed.), vol. 1, Springer, 2007.

[22] Mungan, C. E., "Faraday Isolators and Kirchhoff's Law: A Puzzle," 1999.

[23] Paisley, D. L., "Laser-driven miniature flyer plates for shock initiation of secondary explosives," in *Shock Compression of Condensed Matter* (Schmidt, S. C., Johnson, J. N., and Davidson, L. W., eds.), pp. 733–736, American Physical Society Topical Conference Proceedings, August 1989.

[24] Paisley, D. L., Warnes, R. H., and Stahl, D. B., "Experimental Techniques for Subnanosecond Resolution of Laser-Launched Plates and Impact Studies," tech. rep., Los Alamos National Lab, 1994.

[25] Rice, M. H., McQueen, R. G., and Walsh, J. M., "Compression of Solids by Strong Shock Waves," *Solid State Physics*, vol. 6, pp. 1–63, 1958.

[26] Ripin, B. H., Decoste, R., Obenschain, S. P., Bodner, S. E., McLean, E. A., Young, F. C., Whitlock, R. R., Armstrong, C. M., Grun, J., Stamper, J. A., Gold, S. H., Nagel, D. J., Lehmberg, R. H., and McMahon, J. M., "Laser-plasma interaction and ablative acceleration of thin foils at 10^{12}-10^{15} W/cm^2," *Physics of Fluids*, vol. 23, pp. 1012–1030, 1980.

[27] Robbins, D. L., Stahl, D. B., Sheffield, S. A., Alexander, D. J., Paisley, D. L., Kelly, A. M., Hanrahan, R. J., Snow, R. C., Gehr, R. J., Rupp, R. J., and Bucholtz, S. M., "Laser-Driven Miniflyer System," Tech. Rep. LA-14150, Los Alamos National Laboratory, 2004.

[28] Romero, L. A. and Dickey, F. M., "Lossless Laser Beam Shaping," *Journal of the Optical Society of America*, vol. 13, pp. 751–760, April 1996.

[29] Schmitt, R. L. and Rahn, L. A., "Diode-laser-pumped Nd:YAG laser injection seeding system," *Appl. Opt.*, vol. 25, no. 5, pp. 629–633, 1986.

[30] Shealy, D. L., "Historical perspective of laser beam shaping," in *SPIE The International Society for Optical Engineering Proceedings*, 4770, pp. 28–47, 2002.

[31] Sheffield, S. A., Rogers Jr., J. W., and Castaneda, J. N., "Velocity measurements of laser-driven flyers backed by high impedance windows," in *American Physical Society Topical Conference on Shock Waves in Condenseed Matter* (Gupta, Y. M., ed.), vol. 4, pp. 541–546, Plenum Press, 1985.

[32] Smith, A. V. and Do, B. T., "Picosecond-nanosecond bulk damage of fused silica at 1064nm," in *Laser-Induced Damage in Optical Materials: 2008* (Exarhos, G. J., Ristau, D., Soileau, M. J., and Stolz, C. J., eds.), vol. 7132, SPIE, 2008.

[33] Stahl, D. B., Gehr, R. J., Harper, R. W., Rupp, T. D., Sheffield, S. A., and Robbins, D. L., "Flyer Velocity Characteristics of the Laser-Driven Miniflyer System," *American Physical Society*, 1999.

[34] Strand, O. T., Goosman, D. R., Martinez, C., Whitworth, T. L., and Kuhlow, W. W., "Compact system for high-speed velocimetry using heterodyne techniques," *Review of Scientific Instruments*, vol. 77, no. 8, p. 083108, 2006.

[35] Strand, O. T., Berzins, L. V., Goosman, D. R., Kuhlow, W. W., Sargis, P. D., and Whitworth, T. L., "Velocimetry using heterodyne techniques," in *26th International Congress on High-Speed Photography and Photonics* (Paisley, D. L., Kleinfelder, S., Snyder, D. R., and Thompson, B. J., eds.), vol. 5580, pp. 593–599, SPIE, 2005.

[36] Surelite, "Seeded Surelite Data Sheet," 2006.

[37] Svelto, O., *Principles of Lasers*. Springer Science+Business Media, Inc., 4 ed., 1998. translated from Italian and edited by Hanna, D. C.

[38] Swift, D. C., Niemczura, J. G., Paisley, D. L., Johnson, R. P., Luo, S., and Tierney IV, T. E., "Laser-Launched Flyer Plates for Shock Physics Experiments," *Review of Scientific Instruments*, vol. 76, no. 093907, 2005.

[39] Tollier, L. and Fabbro, R., "Study of the laser-driven spallation process by the visar interferometry technique. ii. experiment and simulation of the spallation process," *Journal of Applied Physics*, vol. 83, no. 3, pp. 1231–1237, 1998.

[40] Trott, W. M., "Studies of laser-driven flyer acceleration using optical fiber coupling," in *Shock Compression of Condensed Matter*, American Physical Society Topical Conference Proceedings, January 1991.

[41] Trott, W. M., "Investigation of the dynamic behavior of laser-driven flyers," in *High-pressure science and technolgy*, vol. 309, pp. 1655–1658, American Institute of Phsyics Conference Proceedings, July 1994.

[42] Trott, W. M. and Meeks, K. D., "High-power nd:glass laser transmission through optical fibers and it's use in acceleration of thin foil targets," *Journal of Applied Physics*, vol. 67, no. 7, pp. 3297–3301, 1990.

[43] Watson, S. and Field, J. E., "Integrity of thin, laser-driven flyer plates," *Journal of Applied Physics*, vol. 88, no. 7, pp. 3859–3864, 2000.